NATIONAL AERONAUTICS AND SPACE ADMINISTRATION

Technical Report 32-1520

Effects of High-Temperature, High-Humidity Environment on Silicon Solar Cell Contacts

Robert K. Yasui
Paul A. Berman

JET PROPULSION LABORATORY
CALIFORNIA INSTITUTE OF TECHNOLOGY
PASADENA, CALIFORNIA

February 15, 1971

NATIONAL AERONAUTICS AND SPACE ADMINISTRATION

Technical Report 32-1520

Effects of High-Temperature, High-Humidity Environment on Silicon Solar Cell Contacts

Robert K. Yasui
Paul A. Berman

JET PROPULSION LABORATORY
CALIFORNIA INSTITUTE OF TECHNOLOGY
PASADENA, CALIFORNIA

February 15, 1971

Prepared Under Contract No. NAS 7-100
National Aeronautics and Space Administration

Preface

The work described in this report was performed by the Guidance and Control Division of the Jet Propulsion Laboratory.

Abstract

The electrical and mechanical characteristics of various solar cell contact systems after exposure to a high-temperature, high-humidity environment were investigated at the Jet Propulsion Laboratory. The results are discussed. An unexpected failure mode involved degradation of the silicon monoxide antireflective coating after environmental exposure. Significant degradation of electrical characteristics was observed in cells having palladium-containing Ti–Ag contacts, and differences in contact structure and composition were noted between different manufacturers. Non-palladium-containing Ti–Ag contacts on lithium-doped cells showed a surprising degree of stability. In general, the most stable contact system, electrically and mechanically, was the solder-coated, Ti–Ag system used on the *Mariner* Mars 1969 solar cells.

Contents

Tables

Figures

Contents (contd)

Figures (contd)

Contents (contd)

Figures (contd)

Contents (contd)

Figures (contd)

Effects of High-Temperature, High-Humidity Environment on Silicon Solar Cell Contacts

I. Introduction

The loss of solar cell contact pull strength after exposure to high-humidity environments has seriously concerned users of photovoltaic power systems (Refs. 1–3). In some cases, the concern has been so great that a protective layer of lead–tin–silver solder has been used over the state-of-the-art titanium–silver solar cell contacts. The solder layer minimizes the detrimental effects of humidity on the solar cell contacts but increases panel weight and, because of the mismatch between the solder, the contact system, and the silicon, reduces the capability of surviving severe thermal shocks (Ref. 2). Therefore, a comprehensive investigation of various contact systems was undertaken at the Jet Propulsion Laboratory (JPL) to determine the electrical and mechanical characteristics of the systems under an environment of high humidity coupled with relatively high temperatures. This report describes the results of an experimental test program conducted in 1969 and 1970 to evaluate seven types of solar cells from three manufacturers.

II. Background

It has been reported that the severe loss of contact strength exhibited by state-of-the-art solar cell titanium–silver contacts is a result of an electrochemical reaction between the titanium and the silver, which is greatly enhanced in the presence of water (Ref. 4). Recent studies by Bishop (Ref. 3) using mass spectroscopy to determine the fundamental mechanisms which cause solar cells with titanium contacts to degrade when stored in humid atmospheres revealed that the most important contaminants were chloride and fluoride ions. The presence of chloride and fluoride ions, even in small concentrations, accelerated degradation of the contacts. Contacts free of halogen contaminants were also found to degrade in humid atmospheres. Another major conclusion reached by Bishop is that the degree and nature of the silver porosity depends on many factors in contact manufacturing, such as substrate temperature, deposition rates, and degree of vacuum during deposition. Atmospheric sulfides may cause tarnishing of the silver layer, an im-

portant factor in determining solderability, welding, and thermocompression joining characteristics.

Theoretical and experimental analysis of possible structures of Ti–Ag and Ti–Pd–Ag solderless solar cell contacts have been made by Becker (Ref. 5). Becker's work was directed toward understanding the structure of the Ti–Ag and Ti–Pd–Ag contacts and factors, either production or environmental, which determine that structure. Becker, like Bishop, found experimentally that the silver film contains defects, probably pinholes, which penetrate the film. Also, palladium appears to be present as an amorphous layer between the silver and the usual Ti + TiH_2 layer, but several of the contacts also exhibited Ti $(Ag, Si)_2$-type alloy. It was noted that normal production contacts oxidize to Ag–TiO_2 (anatase + rutile) silicon contacts after high-temperature, high-humidity exposure and that oxidation occurs locally. These results were measured on sample cells supplied by JPL from the same groups analyzed in this report.

It has been proposed that the addition of palladium to the titanium layer significantly inhibits the corrosive reaction with the silver (Ref. 4). In order to corroborate these results, silicon solar cells with and without the addition of palladium to the titanium layer were purchased by JPL. These cells were of the *n*-diffused into *p*-base silicon (*n* on *p*) configuration with dimensions of 2 cm × 2 cm × 0.045 cm, and were fabricated from crucible-grown silicon having a resistivity of 2 ohm-cm. The cells were basically of the configuration used for the *Mariner* 1969 spacecraft except that in this case there was no solder coating over the contacts. Ten cells of each type were exposed to a relative humidity of 95% and a temperature of 80°C for 192 h while two cells of each type were retained as unexposed controls. After the environmental exposure, tin-plated Kovar[1] test tabs were soldered to the top (*n*) contacts by means of a pulse solder reflow soldering machine, using Alpha 32 solder (97.5% Sn, 2.5% Ag). The tabs were then pulled in an Instron[2] material test machine at a pull rate of 5.03 cm/min (see the Appendix for further details). The results are summarized in Fig. 1.

The contact system incorporating palladium showed no significant decrease in average pull strength as a result of the exposure, while the contact systems without palladium exhibited an average pull strength decrease

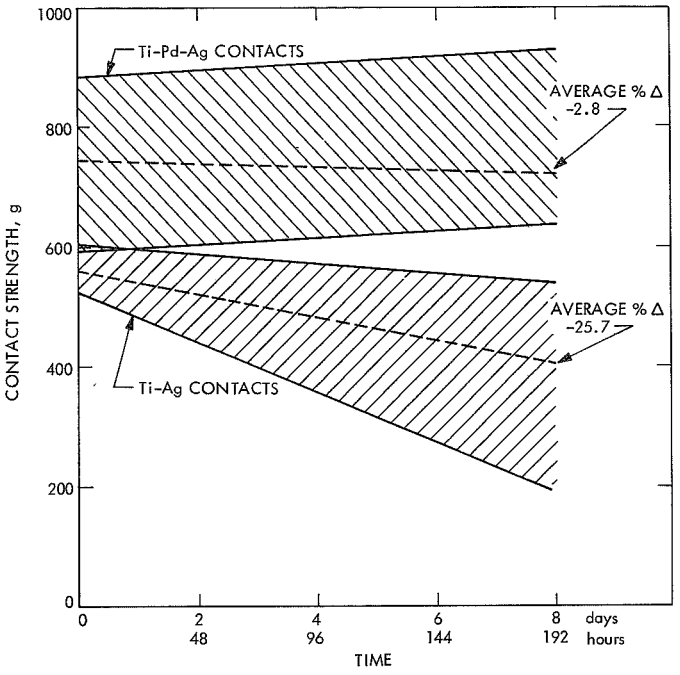

Fig. 1. Effects of high temperature–humidity environment on top (*n*) contact strength of solderless Ti–Pd–Ag silicon solar cells

of approximately 25%. While the spread in contact strength prior to exposure was considerably greater for the palladium-containing system than for the non-palladium-containing system, ranging from 600 to 900 g, the spread after exposure of 192 h remained constant. The pretest contact strengths exhibited by the non-palladium-containing system were much lower, ranging between 500 and 600 g, and the spread after exposure to 192 h increased significantly, ranging between 200 and 550 g. Prior to test, the best non-palladium-containing contact was only as good as the worst palladium-containing contact, and after exposure for 192 h no non-palladium-containing contact had a contact strength as great as the poorest palladium-containing contact.

The results of this experiment indicated that further investigations of the palladium-containing contact system were warranted, and that comparisons not only with the non-palladium system, but also with the solder-coated non-palladium-containing Ti–Ag system used on the *Mariner* Mars 1969 cells would be of great interest.

III. Experimental Investigations

The objective of these investigations was a correlation of the effects of high-temperature, high-humidity envi-

[1]Alloy manufactured by the Westinghouse Electric Co., Pittsburgh, Pa.

[2]Instron Corp., Canton, Mass.

Table 1. Solar cell description

Cell code	Cell vendor	Quantity		Type	Nominal dimensions			Base resistivity ρr_b, ohm-cm	Contact metals
		Test	Control		Size, cm	Thickness			
						Cm	Mils		
H	Heliotek[a]	25	5	n/p	2 × 2	0.045	18	2	Ti–Ag
M	Heliotek	25	5						Ti–Ag, soldered
HP	Heliotek	15	3						Ti–Pd–Ag
CP	Centralab[b]	15	3	n/p	2 × 2	0.045	18	2	Ti–Pd–Ag
TL	Texas Instruments[c]	5	5	Li–p/n (crucible-grown)	1 × 2	0.038	15	20[d]	Ti–Ag
CL	Centralab	5	5	Li–p/n (crucible-grown)	1 × 2	0.038	15	25 to 35[d]	Ti–Ag
HL	Heliotek	5	5	Li–p/n (float-zone)	1 × 2	0.038	15	20[d]	Ti–Ag

[a]Heliotek, a Division of Textron Inc., Sylmar, California.

[b]Centralab, The Electronics Division of Globe-Union, Inc., Milwaukee, Wis.

[c]Texas Instruments Inc., Semiconductor Circuits Division, Dallas, Texas.

[d]Base resistivity prior to introduction of lithium.

NOTE: Basic measurements of solar cell thickness were in mils.

ronments on state-of-the-art and palladium-containing, titanium–silver contacts with respect to both the electrical and the mechanical characteristics of the cells. The solar cells investigated in these experiments (see Table 1) were procured in accordance with minimum acceptance criteria established by JPL for use on flight programs, except for the advanced-development p-diffused into n-base silicon (p on n) lithium-doped cells, which were an exception but were included in this test program to obtain preliminary information on stability under these environments. Because of the small number of samples of lithium-doped cells, measurements were obtained only before and after the total temperature–humidity exposure, rather than at intermediate exposures as was the case with the n on p cells. All cell measurements were compared with data from unexposed control cells throughout the entire test program.

Cell code M represents cells identical to those used on the *Mariner* Mars 1969 program, having a titanium–silver contact with solder coating. The H series represents cells identical to the *Mariner* 1969 cells but without the solder coating, while the HP and CP cells utilize a palladium-containing titanium–silver contact with no solder coating.

The cells' electrical parameters were obtained in the form of current–voltage curves, measured under a Spectrosun X-25L Solar Simulator[3] calibrated to correspond to an air mass zero (AM0) solar intensity of 140 mW/cm^2, by utilizing a variable resistance load and a Hewlett-Packard Model 7030A XY Recorder.[4]

The cells were exposed to an environment of 95% relative humidity at a temperature of 80°C. The exposure times were 240 h (10 days), 480 h (20 days), and 720 h (30 days). At each of these exposure times, five cells of each of the n/p groups were removed from the chamber, electrically measured, and pull tested. Electrical data were tabulated on short circuit current, open circuit voltage, maximum-power current, maximum-power voltage, and maximum power for each of the exposure times and for the unexposed condition. The ratios of these values to the unexposed values were also tabulated. The average value, the standard deviation, and the 95% confidence limits were determined for each of the parameters. Similarly, the contact pull strengths at each of the exposure times for each of the contact system

[3]Spectrolab, a Division of Textron Inc., Sylmar, Calif.

[4]Hewlett-Packard Co., Neely Sales Division, North Hollywood, Calif.

designs were determined, as were the average pull strength, the standard deviation, and the 95% confidence limits. Sample printouts are shown in Tables A-1 through A-3 of the Appendix. In order to further correlate electrical and mechanical characteristics, samples of various types of contact systems were also submitted for analysis utilizing spectrographic techniques.

The conditions of combined high temperature and high humidity investigated here are, in all probability, far in excess of those which would actually be encountered by solar panels in normal use (in the "normal use" case, however, the time involved is of the order of years rather than the 30-day maximum investigated). The high-temperature, high-humidity environments described in this report cannot be interpreted as an "accelerated test," since no functional relationship has yet been established between time of exposure and level of temperature–humidity environment. Furthermore, it has not been determined that the same degradation mechanisms prevail at high temperature–humidity conditions as at more moderate conditions. The levels used in these investigations do, however, represent an extreme environment which should suggest possible failure modes, if they exist. Extreme-level testing has been used in the past by JPL; for example, in acceptance testing of solar cells for *Mariner* Mars 1969, a thermal cycle down to liquid nitrogen temperatures was imposed, although this was far in excess of mission requirements. The cells obtained, however, were exceedingly reliable and satisfied all mission environments (including type-approval tests) without incident. For the high temperature–humidity environments, the interpretation is not quite so simple. It is possible that a contact system which appears to be stable under this extreme environment for relatively short periods of time might exhibit instabilities at lower levels for longer periods of time. Thus the data presented in this report should be used judiciously.

IV. Electrical Test Results

Figure 2 shows the relationship between the short circuit current, normalized to the pretest short circuit current, and the exposure time. (This figure is summarized from the results of Figs. A-1 through A-7 in the Appendix, and compares the results of all contact configurations studied.) All test results for the lithium cells for the 240-h and 480-h exposure times are at best an estimate since, as discussed above, the sample size was large enough only to permit evaluations at the 0 and 720-h exposure time. It can be seen that the HL and CL cells, representing lithium-doped Heliotek float-zone and Centralab lithium-doped crucible-grown cells respectively, exhibit practically no short circuit current degradation after the total exposure time of 720 h. The Texas Instruments lithium-doped crucible-grown cells, TL, exhibited significantly more short circuit current loss and the Heliotek and Centralab cells with palladium-containing contacts exhibited by far the greatest degradation of the short circuit current parameter. Examination of the cells showed very major lifting or removal of the silicon monoxide antireflective coating for cell groups TL, M, H, HP, and CP. The cell groups HL and CL, the Heliotek and Centralab lithium-doped cells, were fabricated utilizing a boron trichloride diffusion source. The fabrication process for these cells is such that an antireflective coating is automatically obtained and hence silicon monoxide antireflective coating for cell groups doped cells was fabricated utilizing a boron tribromide diffusion source which results in a glass layer that is subsequently etched off the surface. This required the deposition of silicon monoxide as an antireflective coating. Cells groups M, H, HP, and CP are all fabricated with the silicon monoxide antireflective coating. Thus, it appears that only the cells having the silicon monoxide antireflective coating exhibited severe short circuit current degradation under these environmental conditions. This was an unexpected and quite disturbing result, over and above the degradation of electrical contacts, and further investigation of the stability of these coatings is indicated. The major loss of short circuit current occurred between 480 and 720 h and, in general, very little degradation was seen prior to the 480-h exposure.

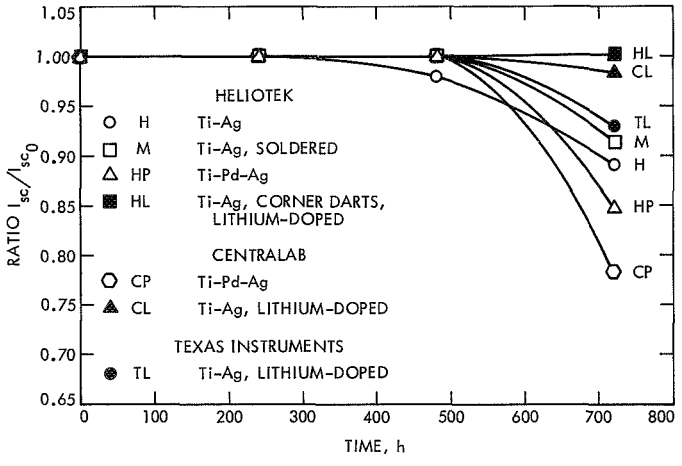

Fig. 2. Relative short circuit current output of silicon solar cells after exposure to high temperature–humidity environment

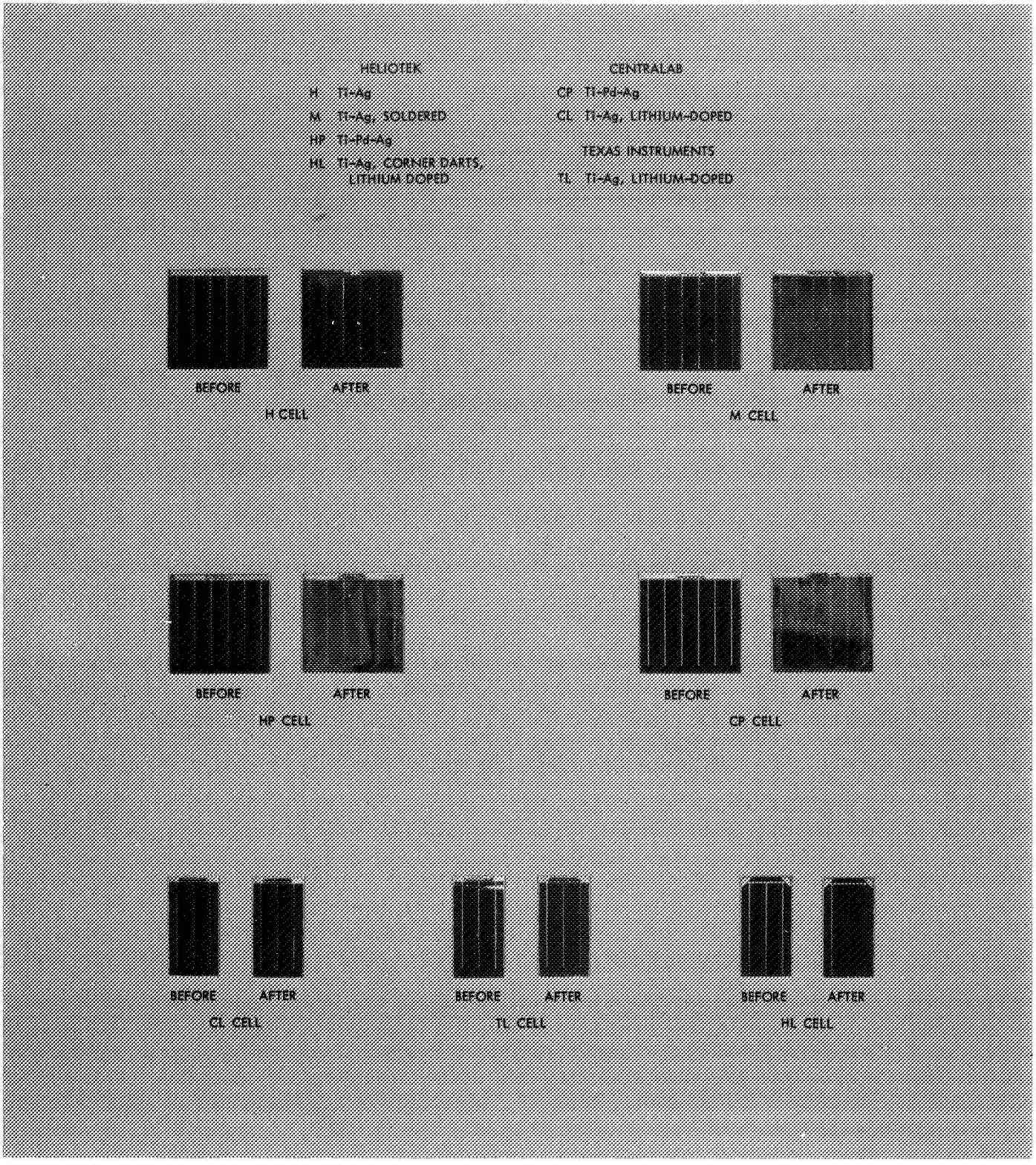

Fig. 3. Comparison between SiO-coated cells before and after 720-h exposure at 95% relative humidity and 80°C

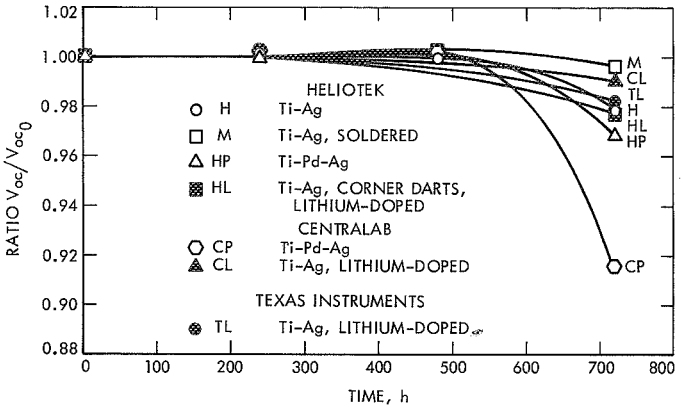

Fig. 4. Relative open circuit voltage of silicon solar cells after exposure to high temperature–humidity environment

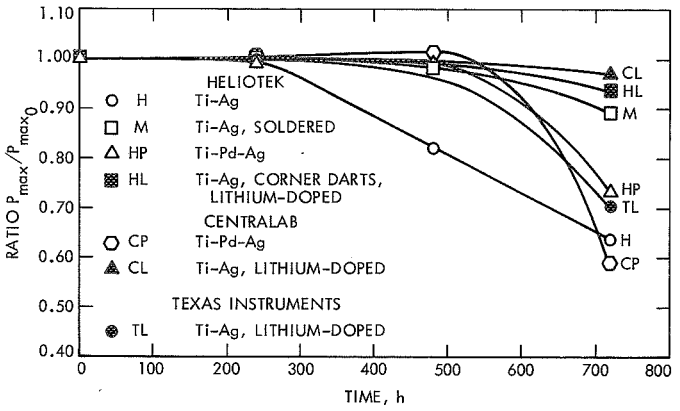

Fig. 5. Relative power output of silicon solar cells after exposure to high temperature–humidity environment

A comparison between cell coatings before and after 720-h exposure is shown in Fig. 3. The coating degradation of the exposed cell is clearly visible.

The open circuit voltage, normalized to the unexposed open circuit voltage, is summarized as a function of exposure time for all test groups in Fig. 4. (The data from which this figure was derived are shown as Figs. A-8 through A-14 in the Appendix). When the open circuit voltage is used as a figure of merit, the relationships between the various cell groups are quite different from the relationships obtained when the short circuit current is used as a figure of merit. In the former, the degradation of silicon monoxide coating is not expected to have a very great effect on the open circuit voltage (although there is a slight reduction in V_{oc} due to the reduced light-generated current), and thus the degradation experienced should be more directly related to actual contact degradation. The cells representative of the *Mariner* Mars 1969 cell configuration, namely, titanium–silver with solder coating, exhibited no significant degradation after the total test time of 720 h. The lithium-doped cells exhibited only minor degradations of about 1 to 2%, as did the H cell group. All these cell groups had the titanium–silver contacts without solder coating. The cell groups exhibiting the greatest degradation of normalized open circuit voltage were those which utilized the palladium-containing, titanium–silver contacts, with the Centralab cells (group CP) exhibiting a degradation of greater than 8%. This latter group showed no significant degradation until after the 480-h exposure time, and all degradation appeared to occur between 480 and 720 h. Thus, the results of the open circuit voltage measurements were, in their own way, as unexpected as the results of the short circuit current measurements, in that the palladium-containing contacts appeared to be more sensitive to the environment than the non-palladium-containing contacts.

The relationship between maximum power, normalized to the unexposed maximum power, and exposure time is shown in Fig. 5. (These curves summarize the results shown in Figs. A-15 through A-21 in the Appendix for all cell groups tested.) Interpretation of Fig. 5 is somewhat difficult due to the two separate degradation mechanisms observed, one being the loss of short circuit current through silicon monoxide deterioration and the other being electrical degradation due to degradation of the cell contacts. It may be concluded, however, that the two lithium-doped cell groups, CL and HL, experienced little degradation in either cell surface characteristics or cell contact characteristics, since the total power degradations were only 3% and 6% for the total duration of the test.

These results might indicate that the addition of lithium, which is of general interest because of its radiation annealing properties, might have an additional benefit in increasing resistance of contacts to high humidity–temperature environments. It should be noted, however, that the TL group of lithium-doped cells exhibited a very severe power degradation of 30%. The reason for this large degradation is almost entirely through loss of the curve power factor, defined as the ratio between the product of maximum power voltage and current to the product of open circuit voltage and short circuit current. The M series of cells, with solder-coated titanium–silver contacts, exhibited a power loss of 11%; however, it should be remembered that a 9% loss was observed in the short circuit current parameter due to silicon monoxide coating degradation. The cells having the palladium-containing contact did not fare

very well from the point of view of maximum power degradation. The HP group showed a degradation of 27% while the CP group suffered 41%, the greatest degradation of all groups tested. Once again, it should be remembered that the CP group suffered a short circuit current degradation of 22%.

As discussed above, detailed statements on the susceptibility of the various contact systems under investigation to degradation in high-temperature, high-humidity ambients are very difficult because of a second major degradation mechanism discovered during the course of these tests, namely, the degradation of the silicon monoxide coating. In general, lithium-doped cells exhibited a surprising degree of stability and the results indicate that further investigations into the use of lithium to enhance humidity resistance of contacts might be warranted. The titanium–silver contact with the solder coating was quite efficient in mitigating the detrimental effects of the high temperature–humidity environment on the electrical characteristics of the contact. Palladium-containing titanium–silver contacts do not appear to be a cure-all for contact problems. There appear to be considerable variations in the effectiveness of the palladium in the contact system in achieving good contact stability. It is suspected that other fabrication parameters (e.g., surface condition, deposition time–temperature profiles, etc.) strongly influence the capability of the palladium to perform this function.

V. Mechanical Test Results

The relative effect of the humidity–temperature environment on the mechanical strength of the contacts was quite different from the results of the electrical stability tests. A summary of the relative contact strength, in percent, as a function of the environmental exposure time for the top contact of the various contact systems is shown in Fig. 6. (The data from which these curves were derived are presented in Figs. A-36 through A-48 in the Appendix.) The pull strength of the top contact of the HL cell group could not be obtained because these cells utilized a corner dart contact configuration which was not compatible with the pull strength test methods used in these experiments (see Appendix.)

For the top contact pull strength tests, the palladium-containing contact systems appear to present a decided advantage over the non-palladium-containing contacts without solder coating. The HP and CP cell groups exhibited a slight increase in pull strength after the 720-h exposure and significant increases at the intermediate test times. The solder-coated titanium–silver contacts, represented by cell group M, also exhibited contact strength increases during the test. Conversely, the TL, H, and CL groups exhibited significant contact strength degradation

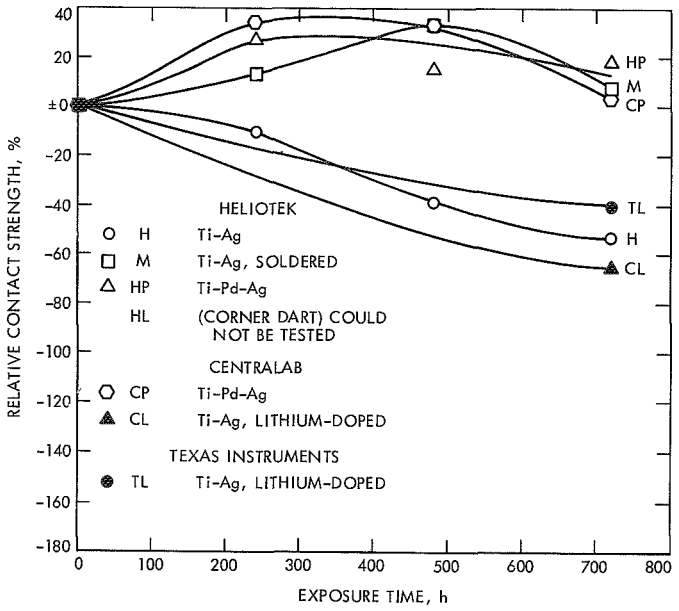

Fig. 6. Effect of high temperature–humidity environment on the contact strength of top-contact silicon solar cells

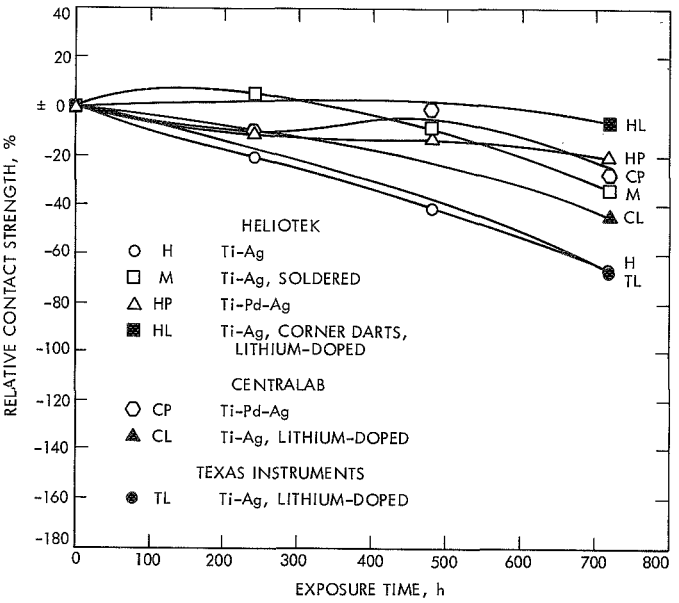

Fig. 7. Effect of high temperature–humidity environment on contact strength of back-contacted silicon solar cells

ranging from −66 to −40% of the pre-exposure value. Furthermore, the effects of the temperature–humidity environment on the contact strengths appear to be a more smoothly varying function of exposure time than the effects on the electrical parameters, where, in general, most of the changes occurred between the exposure times of 480 and 720 h. The CL series of cells exhibited a very severe loss of contact strength on an absolute basis, since the initial strength before exposure was only 453 g. The palladium-containing contacts had initial contact strengths somewhat lower than those of the H and M series cells but were significantly higher after environmental exposure.

A summary of the relative contact strength of the back contact for the various contact systems is shown as a function of exposure time in Fig. 7. (Data were obtained from Figs. A-36 through A-48.) The results of the back-contact pull strength tests are quite different from the results of the top-contact pull strength tests. For the back-contact strength tests, all contact systems exhibited some degree of pull strength degradation. This is in contrast to the results of the top-contact strength tests, which, in some cases, indicated increases in contact pull strength. The loss of pull strength of the HL series is not considered to be significant and is of the order of only 6%. It is unfortunate that because of the corner dart top-contact configuration, pull strength data on the top contact of the HL cells could not be obtained for comparison.

As in the case of the top-contact pull strengths, the cells with the palladium-containing contacts and those having solder-coated contacts fared better than the non-palladium-containing contact cells without solder coating. The exception to this is the previously mentioned HL series which did have non-palladium-containing, non-solder-coated contacts. While the palladium-containing contact cells were, in general, better than the non-palladium-containing cells, the former still exhibited losses in contact strength of greater than 20% after the 720-h exposure. The CL and HL groups of cells exhibited lower contact strengths for the unexposed condition than did the other cell groups, while the solder-coated, non-palladium-containing contact cells (group M) exhibited an extremely high initial contact strength. As is true for the top-contact strength evaluations, the effect of humidity on the contact strength appears to be a smoothly varying function of exposure time, in contrast to the results of the electrical tests, which indicated that most of the degradation occurred during the exposure time between 480 and 720 h.

VI. Metallurgical Evaluation of Contacts

A. Scanning Electron Micrographs

Scanning electron micrographs were made on a number of sample cells. Figure 8a–d shows a set of typical micrographs for the Ti–Pd–Ag contact system, comparing the top and bottom contacts of a Heliotek and a Centralab cell. This figure indicates that the structure of the contacts varies considerably between the top and bottom contact and between the two cell vendors. The difference in back-contact structure is particularly large for the two vendors, as shown in Fig. 8c and d. While the surface of the contact on the Centralab cell appears to present a landscape of hills and valleys, the surface of the Heliotek cell presents a cratered topography. Furthermore, the Centralab cell contact appears to be layered rather than homogeneous, which is interesting since these cells exhibited the greatest electrical degradation as a result of the temperature–humidity test. A similar set of electron micrographs for the Ti–Ag contact system is shown in Fig. 9a–d. Again, the back contacts appear to be structurally quite different for the two manufacturers (Fig. 9c and d), the Centralab and Heliotek cells having a hilly and cratered topography respectively (as was also observed in the Ti–Pd–Ag micrographs). These results indicate that there are significant differences in the surface preparation and the deposition techniques between the two manufacturers.

B. Spectrographic Analysis of Solar Cell Contacts

The spectrographic analysis of solar cell contacts reported here was conducted for JPL by Pacific Spectrochemical Laboratories, Inc., Los Angeles, Calif. Samples were spectrographically analyzed to (1) distinguish the various metals and impurities in cell contacts and (2) determine the effect of temperature–humidity environment on the composition of Ti–Pd–Ag contacts. Two methods were used to remove the contacted metals from the silicon wafer: (1) scraping the metal contact from the cell and (2) chemical treatment to dissolve the contacts. The contacts in the latter methods were chemically dissolved in a solution of HCl and HNO_3. The analysis was made on the remaining residue. The samples were then placed in a graphite electrode and burned to completion with a direct current arc source. The densities of the resulting lines on the spectrogram were subsequently observed on a densitometer. The spectrograph had a resolution of 6.9Å/mm and is manufactured by the Applied Research Laboratories in Los Angeles, Calif.

For these samples the accuracy was stated to be about 10% on a relative basis and about 20% of the true

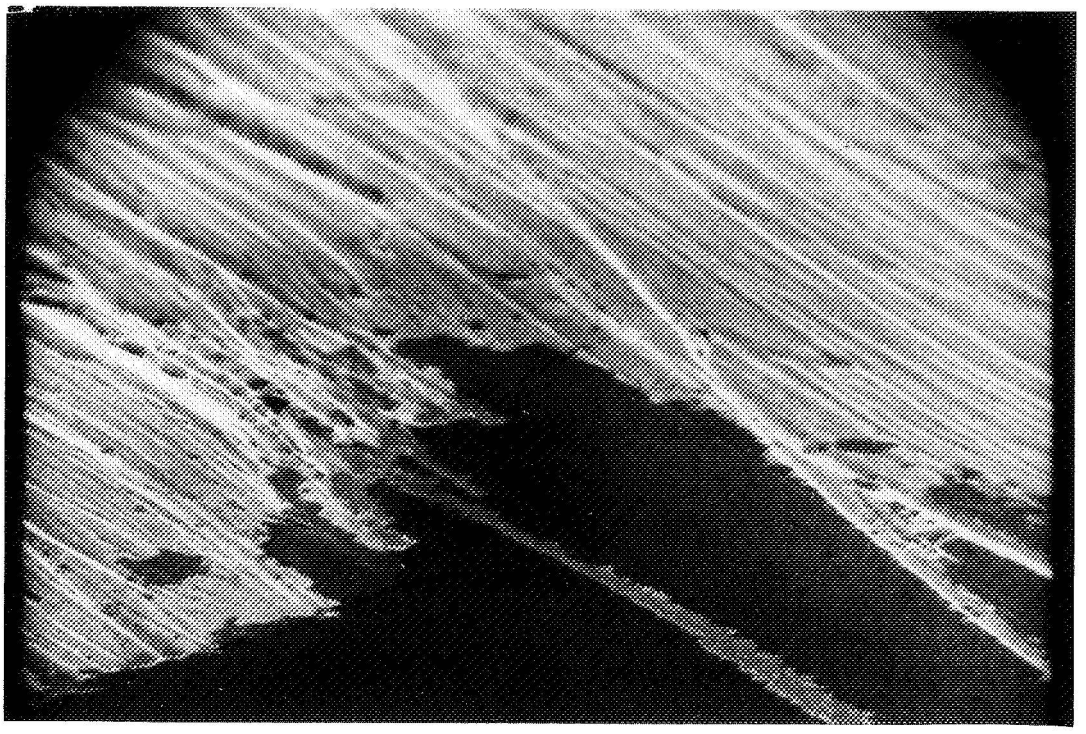

Fig. 8a. Scanning electron micrograph of intersection between top contact and grid of a Centralab solar cell having Ti–Pd–Ag solderless contacts (3600×)

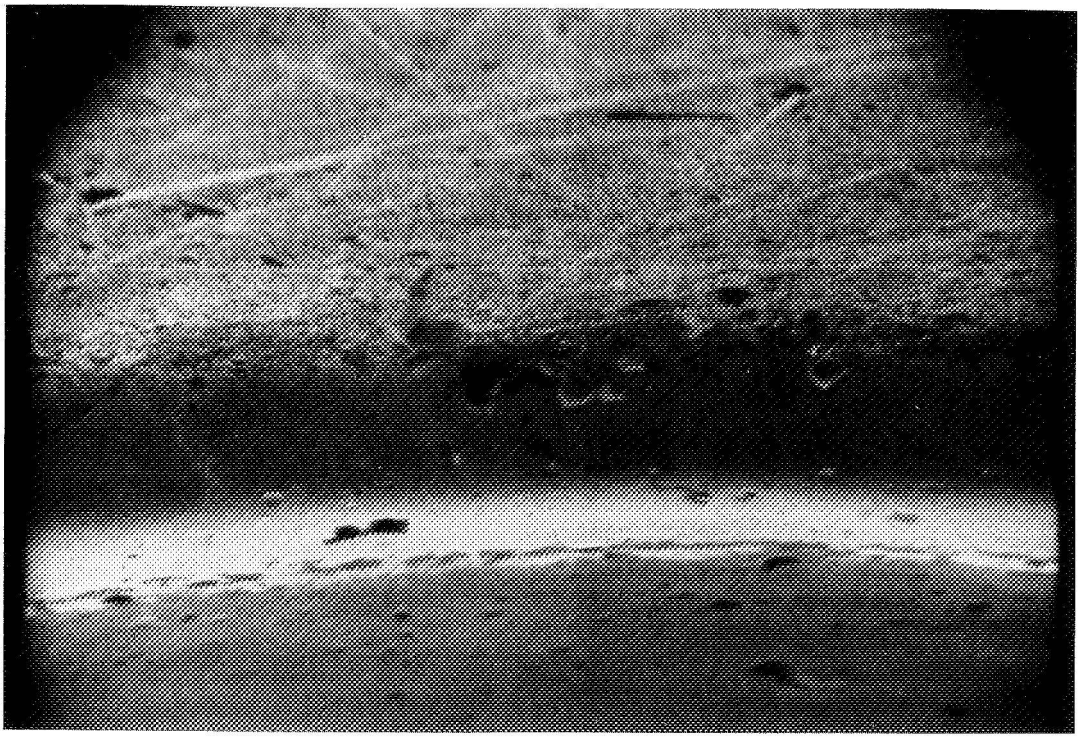

Fig. 8b. Scanning electron micrograph of intersection between top contact and grid of a Heliotek solar cell having Ti–Pd–Ag solderless contacts (4000×)

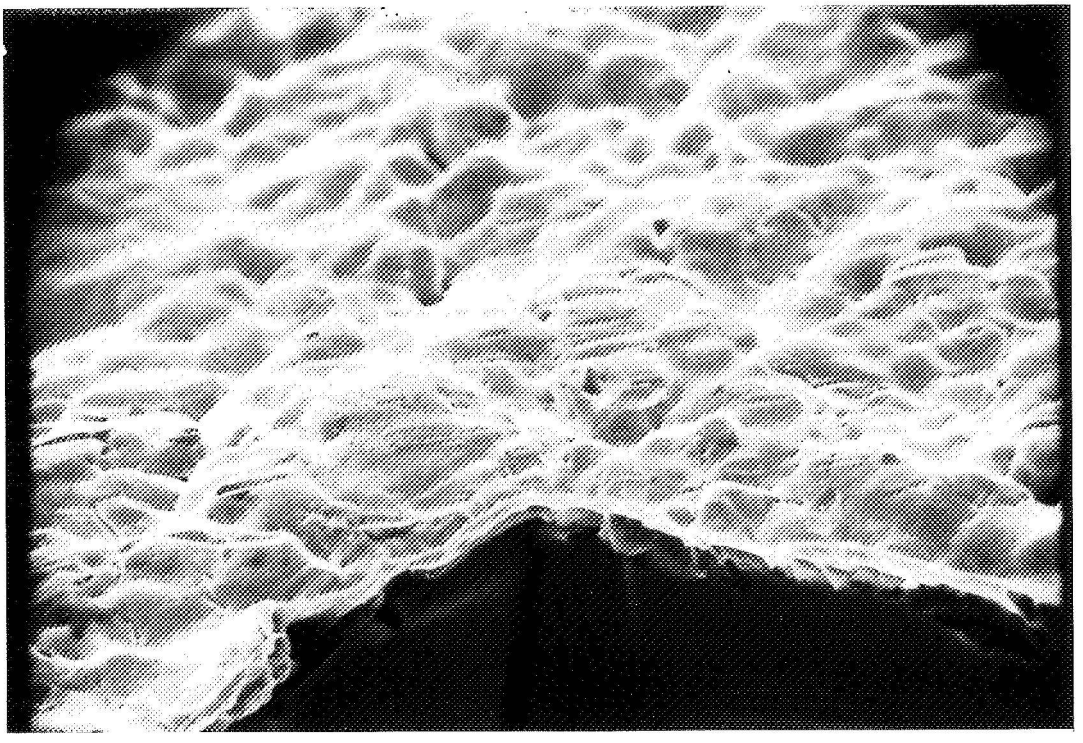

Fig. 8c. Scanning electron micrograph of fracture interface of silicon and back contact of a Centralab solar cell having Ti–Pd–Ag solderless contacts (5200×)

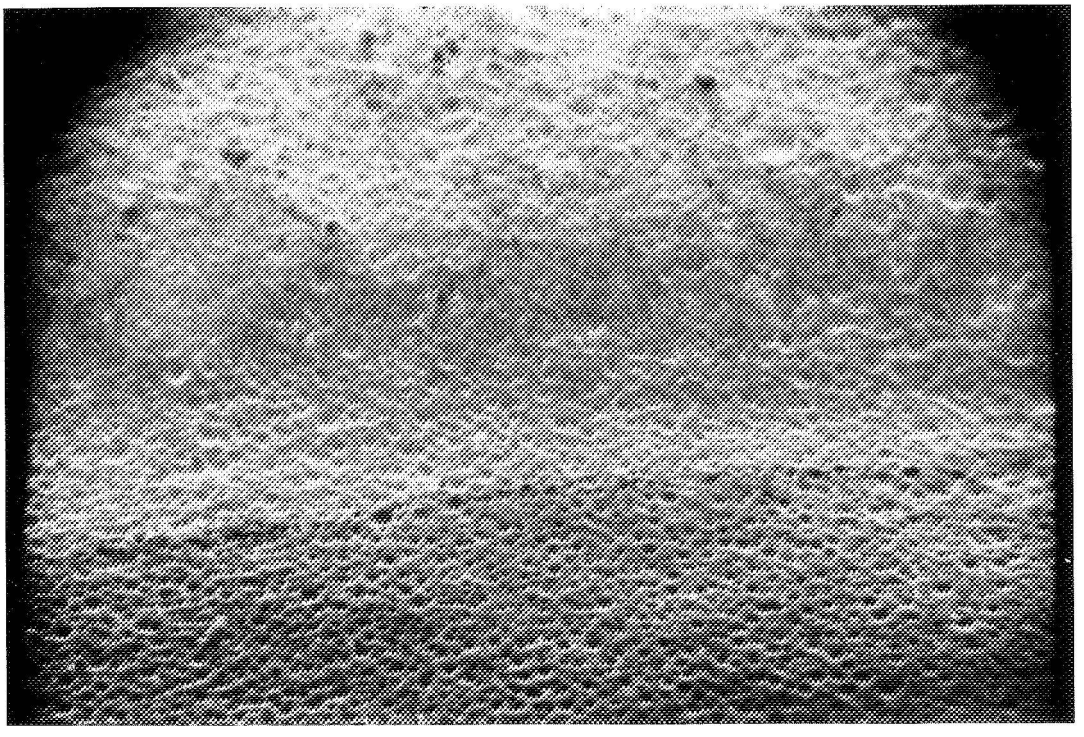

Fig. 8d. Scanning electron micrograph of back-contact surface characteristics of a Heliotek solar cell having Ti–Pd–Ag solderless contacts (4600×)

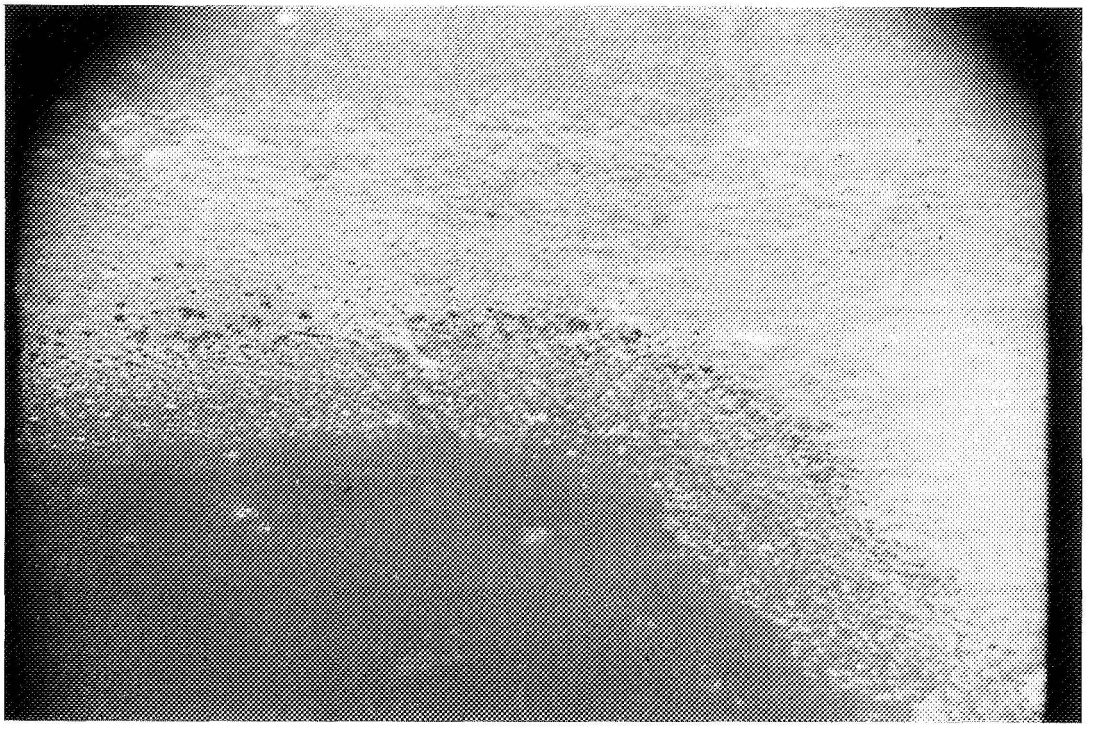

Fig. 9a. Scanning electron micrograph of intersection between top contact and grid of a Centralab solar cell having Ti–Ag solderless contacts (3800×)

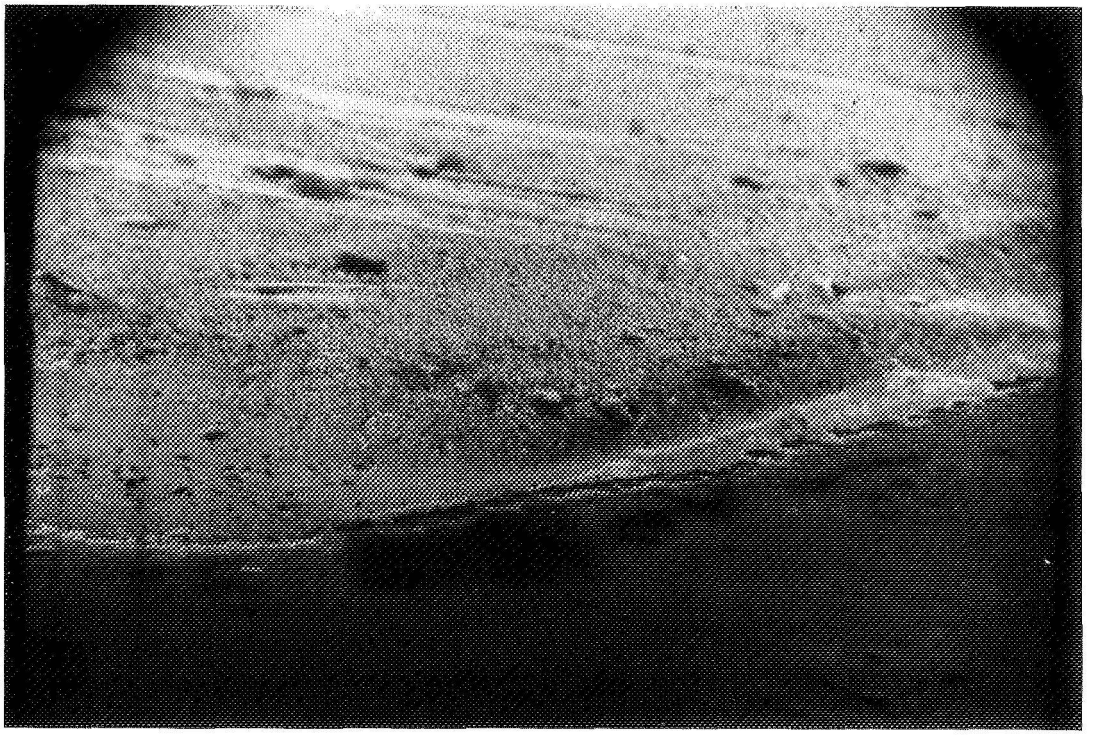

Fig. 9b. Scanning electron micrograph of top contact and light-sensitive surface of a Heliotek solar cell having Ti–Ag solderless contacts (4600×)

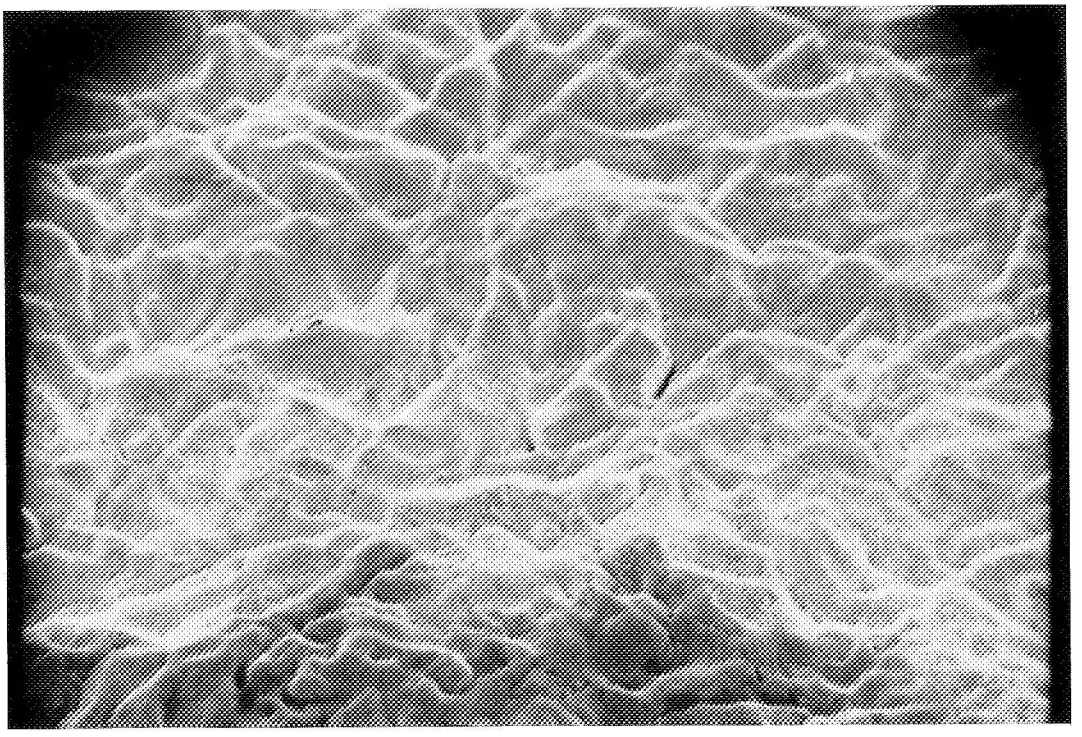

Fig. 9c. Scanning electron micrograph of back-contact surface characteristics of a Centralab solar cell having Ti–Ag solderless contacts (4500×)

Fig. 9d. Scanning electron micrograph of back contact and exposed silicon surface of a Heliotek solar cell having Ti–Ag solderless contacts (3800×)

Table 2. Percentage of palladium as determined by spectrographic analysis on Ti–Pd–Ag contact cells

Sample	Manufacturer	Contact location	Percentage of palladium (relative)
CP-19	Centralab	Top	0.29
CP-19		Bottom	1.6
CP-21		Top	1.3
CP-21	Centralab	Bottom	3.4
HP-46	Heliotek	Top	Nil
HP-46		Bottom	0.032
HP-50		Top	Nil
HP-50	Heliotek	Bottom	0.37
CP-21	Centralab	Bottom	1.3[a]
HP-53	Heliotek	Bottom	0.071[a]

[a]Bottom contact dissolved in HCl, HNO_3 and residue removed.

amount on an absolute basis. Spectrographic results indicate that large amounts of impurities are incorporated into cell contacts. Although it is not clear to what extent these impurities affect contact integrity and performance, it is clear that further study is warranted. In particular, the diffusion characteristics of these various impurities should be considered, since most Ti–Ag contacts are sintered at temperatures on the order of 600°C. There were very significant differences in the percentage amount of palladium incorporated into the contacts, both between the two manufacturers and between the top and bottom contacts, as summarized in Table 2. In general, the Centralab contacts had much higher percentages of palladium than the Heliotek contacts (in some cases there was no indication of palladium in the Heliotek contacts) and the bottom contacts contained higher percentages of palladium than the top contacts.

C. Intrepretation

These investigations indicated several distinct differences in the nature of the contacts as fabricated by the two manufacturers and between the top and bottom contact, particularly with respect to the topography, the percentage amount of palladium, and the percentage amount of impurities such as copper, iron, and gold. It is felt that the effects of the observed variations of these parameters on the resultant cell electrical and mechanical performance in space-type environments should be investigated in order to determine the degree of control required to optimize the contact system for use in the environments of interest. Lack of this information renders evaluation of the Ti–Pd–Ag system, per se, impossible, since it is not known whether the observed degradations are due to an inherent mechanism or rather due to some deficiency in processing.

VII. Conclusions

In general, as previously observed (Ref. 2), the results of electrical tests and of mechanical tests performed on cells exposed to temperature–humidity environments are not always correlatable. Cells that exhibit significant losses in electrical characteristics may not exhibit severe losses in contact strength, while cells that exhibit little or no losses in electrical power may exhibit severe losses of contact strength.

Interpretation of the results of the electrical measurements was confused by an unexpected degradation mechanism: a degradation of the silicon monoxide antireflective coating which resulted in considerable loss of short circuit current, probably due to increased reflection losses. This degradation mechanism certainly warrants further investigation.

From the results of these investigations it appears that the addition of palladium to the titanium–silver contact is not a panacea for degradation of cell characteristics in a high temperature–humidity environment. The loss of open circuit voltage and maximum power was quite considerable for the palladium-containing cells, while it appears that some advantage over the unsoldered non-palladium-containing contacts exists from the point of view of mechanical strength. Significant differences in the structure of the cells with palladium-containing contacts were noted when microphotographs of cells from each of the vendors were examined. Furthermore, spectrographic analysis of the contact systems indicated a much larger percentage of palladium in the Centralab contacts than was found in the Heliotek contacts. It is likely that further control in the amount of palladium and the deposition techniques of palladium-containing contacts will be needed for these contact systems to utilize their full potential.

In general, from the point of view of both electrical and mechanical integrity, solder-coated titanium–silver contacts appear to give the most desirable and consistent results for the high-humidity, high-temperature environments investigated here.

Appendix
Environmental Test Facility, Procedure, and Data

I. Temperature–Humidity Tests

The temperature–humidity environmental tests described in this report were conducted in a Conrad Model FD 32-5-S test chamber,[5] which produces a humid condition by means of a steam-generating system in which moisture is admitted to the chamber in the form of low-pressure steam. A relative humidity of 95% was maintained by a programmable cam in which both the dry bulb temperature and the wet bulb temperature are independently controlled from cam disks cut to produce a predetermined succession of temperatures. As these two cams rotate, at any one moment a dry bulb temperature is produced concurrently with a wet bulb temperature in the test chamber, which yields the desired relative humidity. The test specimens (solar cells) were placed on Teflon-coated metal screen cages adjacent to the wet bulb and dry bulb humidity instruments. To minimize water condensation on the test samples, an inverted V-shaped shield was installed between the test specimens and the top of the chamber. The temperature of 80 ± 2°C was maintained by using a proportional temperature controller and was monitored by means of Leeds and Northrup Model Speedomax G temperature strip chart recorders.[6] The test specimen heat source was provided by Inconel-sheathed electrical heaters. The dehumidifying operation was controlled to minimize water condensation on the test specimens by employing a refrigeration coil, which is located under the work deck at the floor of the chamber. This coil is fed refrigerant when the dehumidifying solenoid is in the open mode. When the coil cools below the dew point in the chamber, moisture condenses onto the coil. As the coil is brought below the freezing point of water, the moisture is trapped or collected on the cooled coil as frost. When the dehumidifying period is completed the frost is melted off the coil and the precipitated water is then drained out of the chamber.

II. Solar Simulation

The illumination source used throughout this test program was a Spectrolab Model X25L close-filtered solar simulator. This simulator uses 19 lenticular lenses in the optical system; these lenses filter and uniformly distribute a relatively collimated light beam at specific distances from a 2.5-kW short arc xenon lamp so that the resultant spectral distribution approaches that of space sunlight. The light beam provides a 30.5-cm-diameter beam pattern having a uniformity of approximately $\pm 2\%$ at the test plane and an illumination level of 140 mW/cm^2 (one solar constant). All solar cells measured under the solar simulator were measured at 140 mW/cm^2 and a test temperature of 28 ± 1°C. The solar intensity and spectral integrity of the solar simulator are constantly monitored and maintained in conjunction with the NASA/JPL solar cell standardization program.

III. Contact Strength Tests

Special contact strength test tabs were standardized for this test program. Tinned, plated, photo-etched Kovar (iron, nickel, and cobalt alloy) tabs 0.01 cm thick were selected for use in evaluation of the subject cells. Each test tab is pre-bent in a forming fixture at a 90-deg angle prior to soldering the cells. The soldering operation is accomplished semiautomatically by use of a Sippican Model RS-333 reflow soldering system.[7] A solder preform (62% Sn, 36% Pb and 2% Ag) was used on all solar cells that were not solder-coated. The solder joint area, assuming an additional area of about 10% for the solder fillet, was calculated to be 0.034 cm^2. To minimize electrode heating during the soldering reflow operation, the soldering time–temperature profile or heat cycle was pulsed twice at a reduced voltage and pulse width to obtain consistent and uniform soldering. An applied electrode pressure of 0.68 kg was used and a total elapsed time of about 4 s for each soldering operation was maintained. This soldering technique was developed to minimize the effects of soldering variations which normally exist when soldering with hand soldering processes. Prior to the initiation of contact strength testing and solder attachment of the test tab and after each temperature/humidity exposure, each cell is visually inspected under 10× magnification.

[5]Conrad Co., Holland, Mich.

[6]Leeds and Northrup Corp., North Wales, Pa.

[7]Sippican Corp., Industrial Products Division, Mattapoisett, Mass.

The contact strength test was conducted by use of an Instron Universal Material Test Machine, Model TM-1,[8] and a self-contained portable temperature control chamber. A special test fixture was developed to adapt to the testing machine so that cells of varying dimension could be mounted and properly aligned perpendicular to the direction of the applied load. A copper-constantan thermocouple is mounted between the test specimen and the test fixture so that cell temperature can be monitored and maintained at ambient laboratory conditions of about 25°C throughout the test.

The top and bottom contact strength of all cells were investigated, except for the top contacts of the HL lithium-doped types. (The HL top contacts were not tested because they have a corner-dart top contact configuration, whereas the other cells all had the conventional bar contact.) The contacts were pulled at a constant rate of 5.03 cm/min until complete separation occurred.

The resultant contact strength was recorded on a strip chart recorder in a form of a stress–strain characteristic curve to the point of separation. At this point the test specimens were reinspected to determine the interfacial characteristics that lead to the separation (e.g., solder failure, contact delamination, broken cell, defective tab, etc.).

[8]Instron Engineering Corp., Long Beach, Calif.

IV. Test Results

Examples of the test data printouts are shown in Tables A-1 through A-3. Table A-1 is a printout of the maximum power for five M-type solar cells after exposure to 80°C and 95% relative humidity for 720 h. Table A-2 is a summary printout for the M-type cells showing changes in short circuit current I_{sc}, open circuit voltage V_{oc}, current at maximum power I_{mp}, voltage at maximum power V_{mp}, and maximum power $P_{\max}$ as a function of exposure time. The average value, 95% confidence limits, and standard deviation of each of these parameters are given for each exposure time. Table A-3 is a summary sheet printout similar to Table A-2, except that all values have been normalized to the values obtained for the unexposed group.

For all figures in the Appendix, the error bars represent the 95% confidence limits and the dots indicate the average values obtained. The curves represent a polynomial fit to the mean values. Figures A-1 through A-7 show the relationship between the short circuit current and the 80°C 95% relative humidity exposure time for each of the cell types investigated. The relationships for V_{oc}, $P_{\max}$, I_{mp}, and V_{mp} are shown as Figs. A-8 through A-14, A-15 through A-21, A-22 through A-28, and A-29 through A-35 respectively. The relationships between contact strength and exposure time at 80°C and 95% relative humidity for each of the cell types are shown in Figs. A-36 through A-48.

References

1. Luft, W., McCraven, C. C., and Aroian, L. A., "Temperature and Humidity Effects on Silicon Solar Cells," in *Conference Record of the Seventh Photovoltaic Specialists Conference*, held in Pasadena, Calif., Nov. 1968. Institute of Electrical and Electronics Engineers, 345 East 47th St., New York.
2. Moss, R., and Berman, P., *Effects of Environmental Exposures on Silicon Solar Cells*, Technical Report 32-1362. Jet Propulsion Laboratory, Pasadena, Calif., Jan. 15, 1969.
3. Bishop, C. J., *Investigation Into the Mechanism of Degradation of Solar Cells With Silver Titanium Contacts*, Final Report. The Boeing Company, Seattle, Wash., July 1, 1970.
4. Fischer, H., and Gereth, R., "New Aspects for the Choice of Contact Materials for Silicon Solar Cells," in *Conference Record of the Seventh Photovoltaic Specialists Conference*, held in Pasadena, Calif., Nov. 1968. Institute of Electrical and Electronics Engineers, 345 East 47th St., New York.
5. Becker, W. H., *The Formation and Degradation of Titanium–Silver Solar Cell Contacts*, Ph.D. Thesis, University of Pennsylvania, Philadelphia, Pa., 1970.

Table A-1. Maximum power, five M-type solar cells

TEST INTERVAL - 720.0

MAXIMUM POWER (PMAX,MW)

90 DEG C AND 95 PCT REL HUMIDITY — 140.0MW/CM2 AND 28 DEG C

HEK N/P 62 2X2 18 STL AG-TI-SOLDER — BAR CONTACTS — TYPE M

CONTROL CELLS	CELL NO.	PRE-TEST	TEST DATA	DEVIATION
	26	60.4584	60.1353	-.3231
	27	59.5270	59.8881	.3611
	28	61.1325	60.5775	-.5550
AVERAGE		60.3726	60.2003	-.1723

CELL NO.	PRE-TEST	TEST DATA	CORR. DATA	CORR./PRE-TEST	% CHANGE
21	59.8263	53.3162	53.4886	.9093	-9.07
22	58.6744	56.4213	56.5936	.9613	-3.87
23	60.9951	54.5968	54.7692	.8979	-10.21
24	61.3126	52.2775	52.4499	.8555	-14.45
25	60.6375	51.2688	51.4411	.8483	-15.17
AVERAGE	59.9151	53.5761	53.7485	.8944	-10.56
95 P.C. CONF. LIMITS	.4548	2.4995	2.4995	.0567	5.67
STANDARD DEVIATION	.8211	2.0134	2.0134	.0457	4.57

Table A-2. Summary of electrical test results for five M-type solar cells

SUMMARY SHEET — SOLAR CELL PARAMETER

TIME/CYCLE		ISC (MA)	VOC (MV)	IMP (MA)	VMP (MV)	PMAX (MW)
	AVERAGE	135.1400	591.0666	122.8533	487.7000	59.9151
.0	95 P.C. CONF. LIMITS	.7059	1.4553	.6950	2.7128	.4548
	STANDARD DEVIATION	1.2746	2.6277	1.2548	4.8983	.8211
	AVERAGE	135.1467	590.9666	123.4467	484.4333	59.8025
240.0	95 P.C. CONF. LIMITS	2.6312	2.1946	1.5836	3.8371	.7521
	STANDARD DEVIATION	2.1194	1.7678	1.2756	3.0908	.6058
	AVERAGE	135.2667	593.2467	123.0733	478.5667	58.9027
480.0	95 P.C. CONF. LIMITS	1.3514	4.3862	.7685	11.3564	1.4775
	STANDARD DEVIATION	1.0886	3.5009	.6190	9.1476	1.1901
	AVERAGE	123.6067	588.5600	111.9800	480.2333	53.7485
720.0	95 P.C. CONF. LIMITS	6.6674	.6436	5.8325	3.4679	2.4995
	STANDARD DEVIATION	5.3706	.5184	4.6981	2.7934	2.0134

Table A-3. Summary of electrical test results for five M-type solar cells, normalized to values for unexposed cells

SUMMARY SHEET RATIO - CORRECTED/PRETEST

TIME/CYCLE		ISC/ISCO	VOC/VOCO	IMP/IMPO	VMP/VMPO	PMAX/PMAX
	AVERAGE	1.0000	1.0000	1.0000	1.0000	1.0000
.0	95 P.C. CONF. LIMITS	.0000	.0000	.0000	.0000	.0000
	STANDARD DEVIATION	.0000	.0000	.0000	.0000	.0000
	AVERAGE	.9997	.9995	1.0070	.9942	1.0011
240.0	95 P.C. CONF. LIMITS	.0073	.0011	.0098	.0087	.0164
	STANDARD DEVIATION	.0059	.0009	.0079	.0070	.0132
	AVERAGE	1.0012	1.0033	1.0031	.9806	.9838
480.0	95 P.C. CONF. LIMITS	.0029	.0013	.0106	.0149	.0246
	STANDARD DEVIATION	.0023	.0011	.0085	.0120	.0198
	AVERAGE	.9147	.9965	.9086	.9846	.8944
720.0	95 P.C. CONF. LIMITS	.0481	.0030	.0504	.0155	.0567
	STANDARD DEVIATION	.0387	.0025	.0406	.0125	.0457

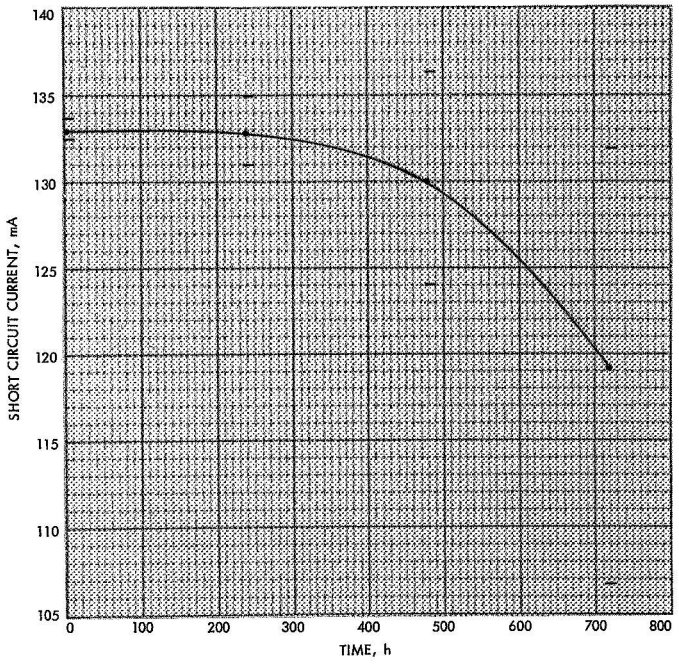

Fig. A-1. Short circuit current as a function of exposure time, H cells (Heliotek Ti–Ag, solderless)

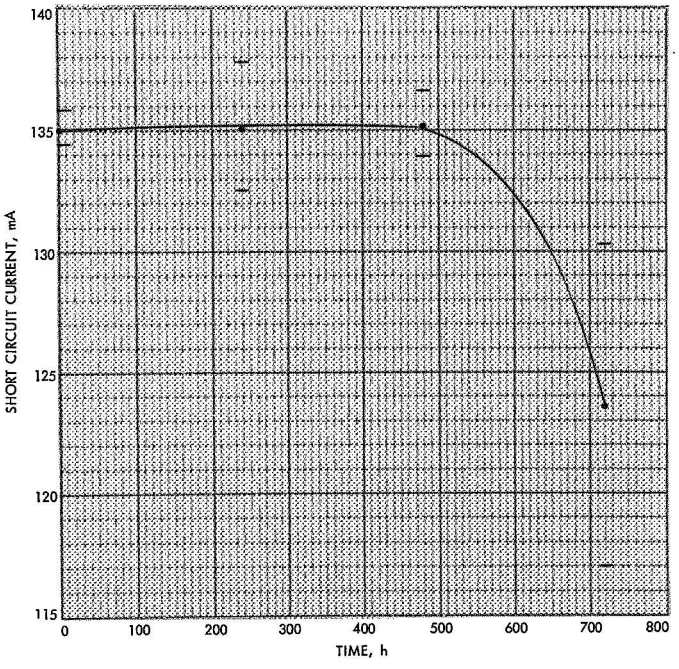

Fig. A-2. Short circuit current as a function of exposure time, M cells (Heliotek Ti–Ag, soldered)

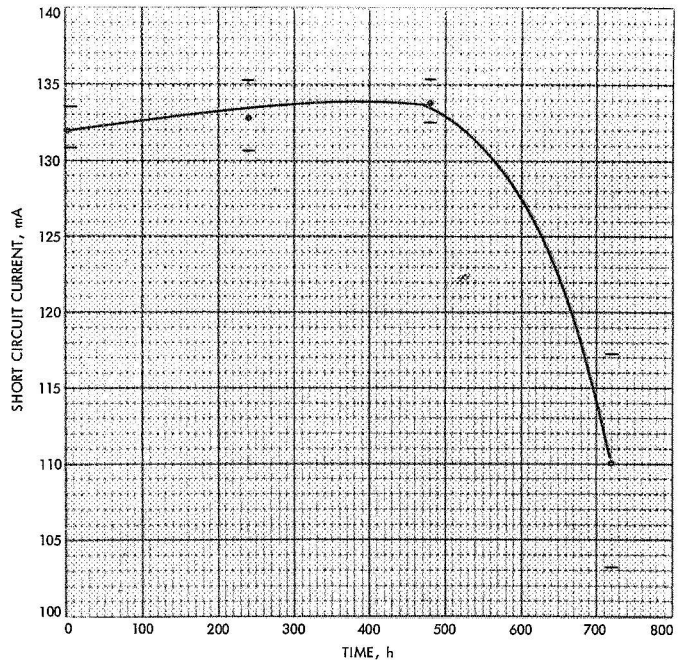

Fig. A-3. Short circuit current as a function of exposure time, HP cells (Heliotek Ti–Pd–Ag, solderless)

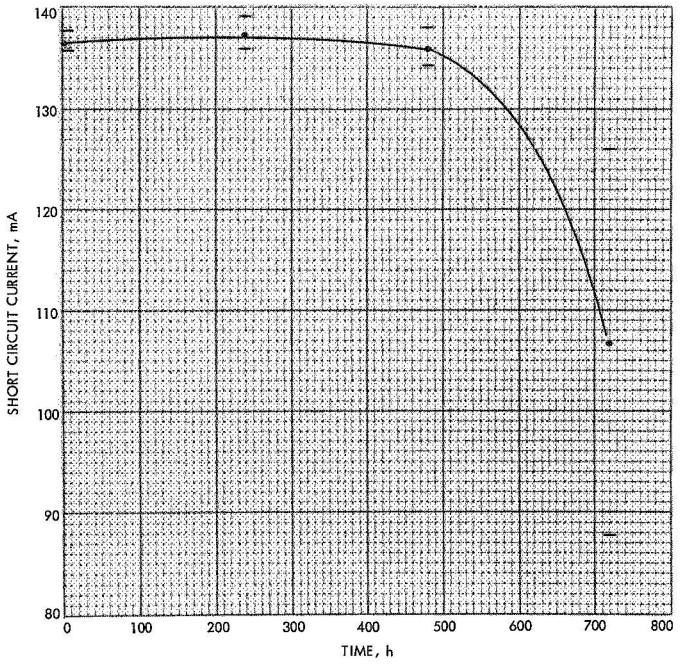

Fig. A-4. Short circuit current as a function of exposure time, CP cells (Centralab Ti–Pd–Ag, solderless)

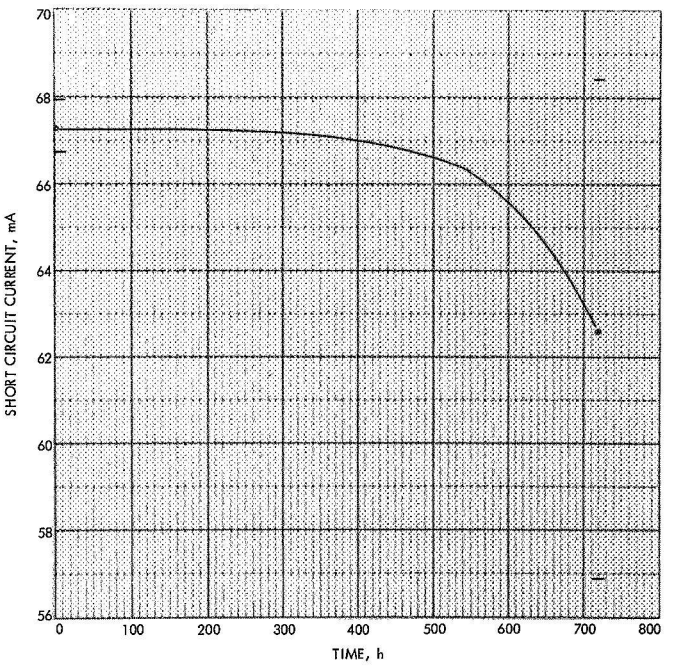

Fig. A-5. Short circuit current as a function of exposure time, TL cells (Texas Instruments Ti–Ag, solderless, lithium-doped)

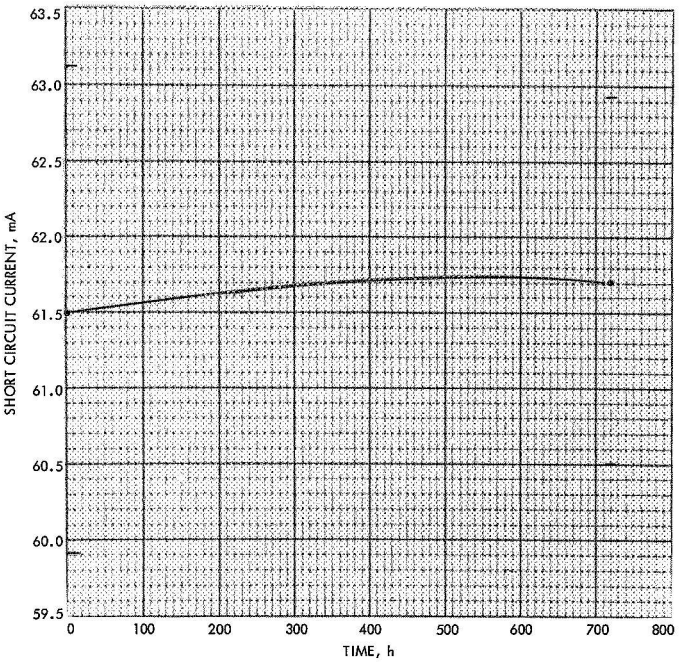

Fig. A-6. Short circuit current as a function of exposure time, HL cells (Heliotek Ti–Ag solderless corner dart contacts, lithium-doped)

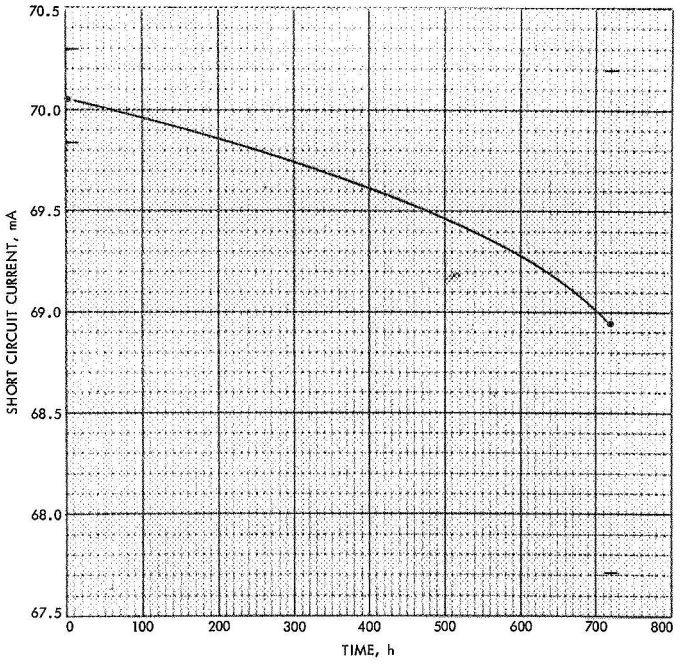

Fig. A-7. Short circuit current as a function of exposure time, CL cells (Centralab Ti–Ag solderless, lithium-doped)

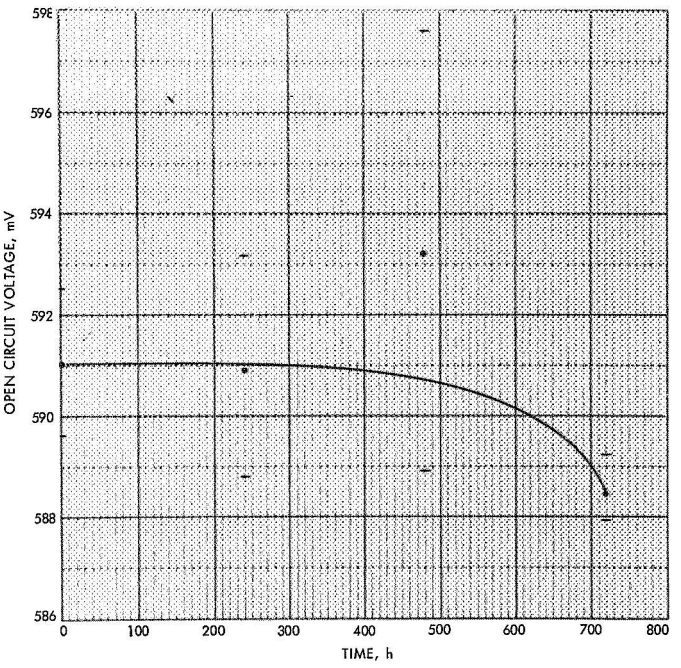

Fig. A-9. Open circuit voltage as a function of exposure time, M cells (Heliotek Ti–Ag, soldered)

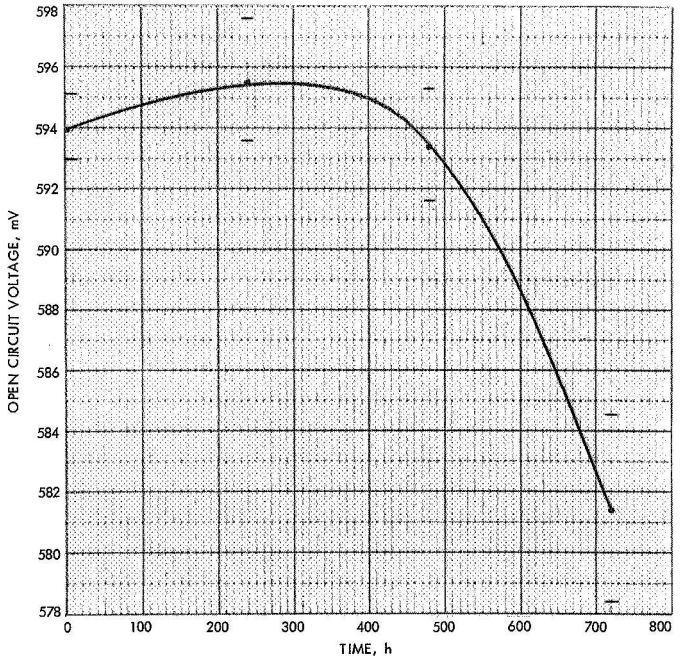

Fig. A-8. Open circuit voltage as a function of exposure time, H cells (Heliotek Ti–Ag, solderless)

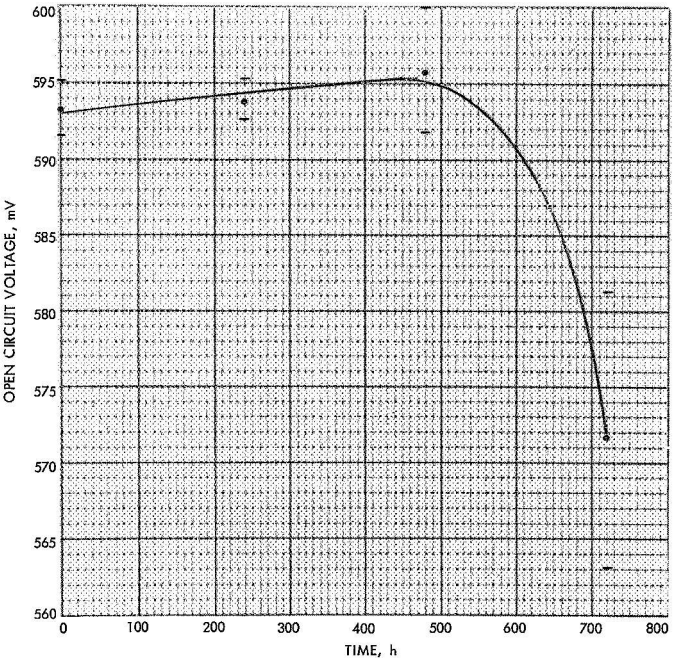

Fig. A-10. Open circuit voltage as a function of exposure time, HP cells (Heliotek Ti–Pd–Ag, solderless)

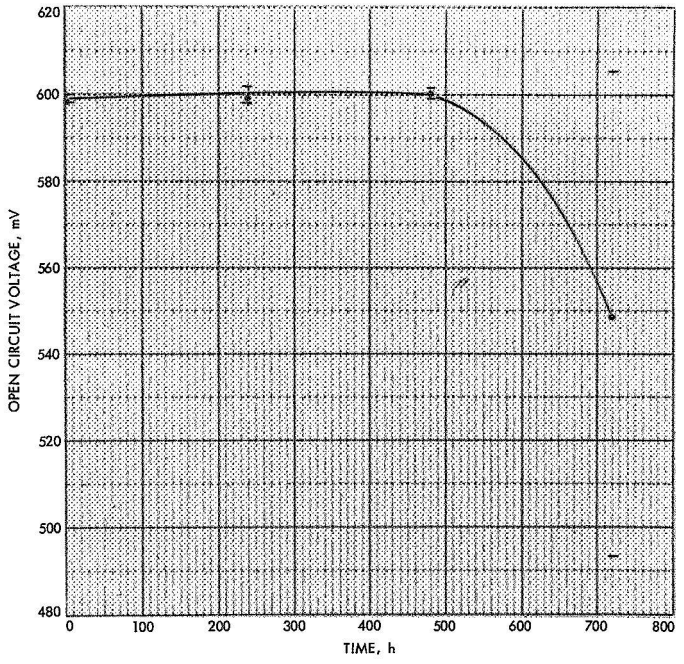

Fig. A-11. Open circuit voltage as a function of exposure time, CP cells (Centralab Ti–Pd–Ag, solderless)

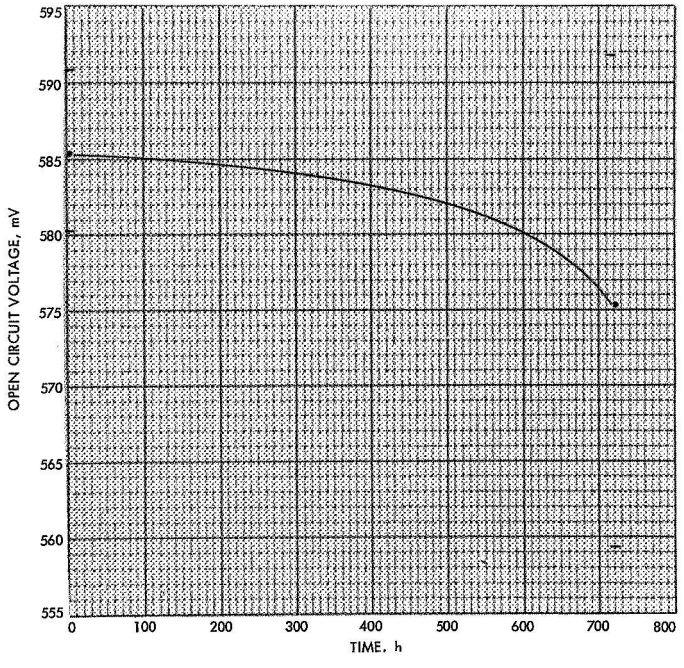

Fig. A-12. Open circuit voltage as a function of exposure time, TL cells (Texas Instruments Ti–Ag, solderless, lithium-doped)

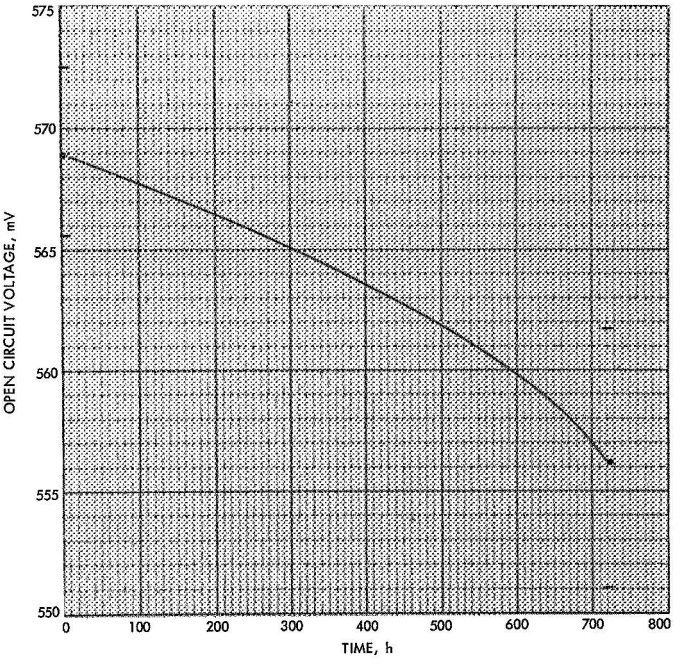

Fig. A-13. Open circuit voltage as a function of exposure time, HL cells (Heliotek Ti–Ag, solderless corner dart contacts, lithium-doped)

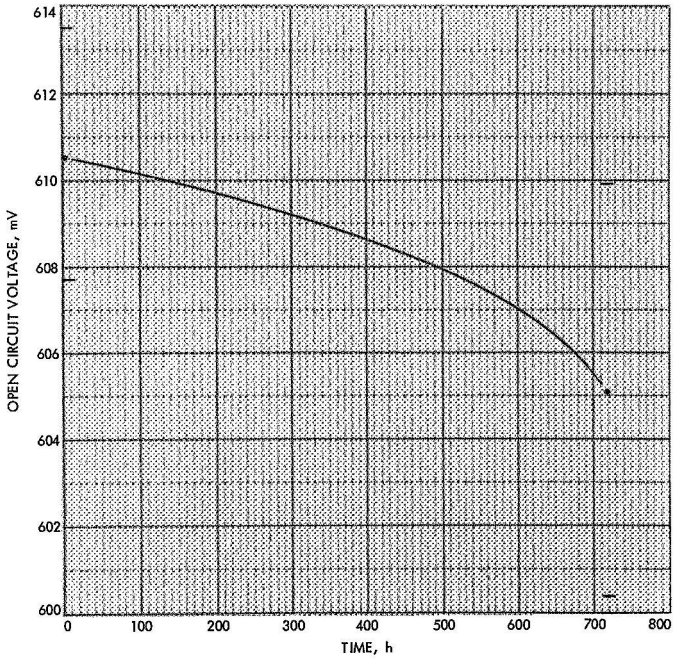

Fig. A-14. Open circuit voltage as a function of exposure time, CL cells, Centralab Ti–Ag, solderless, lithium-doped)

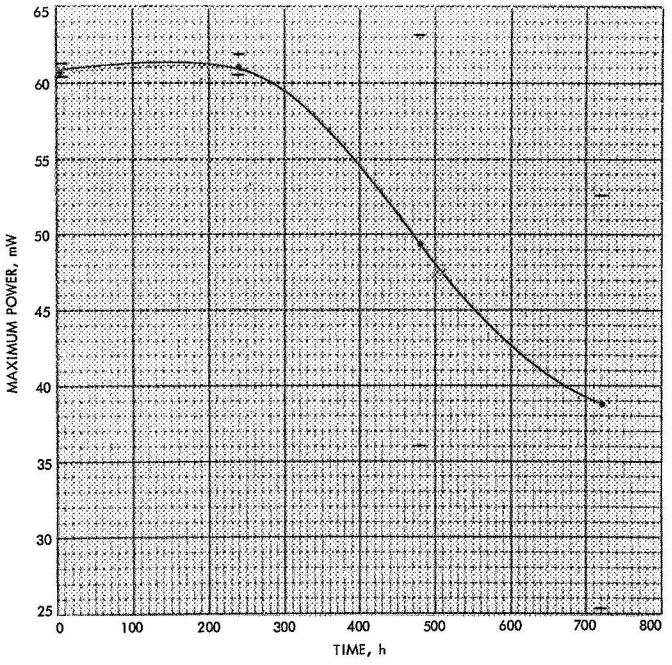

Fig. A-15. Maximum power as a function of exposure time, H cells (Heliotek Ti–Ag, solderless)

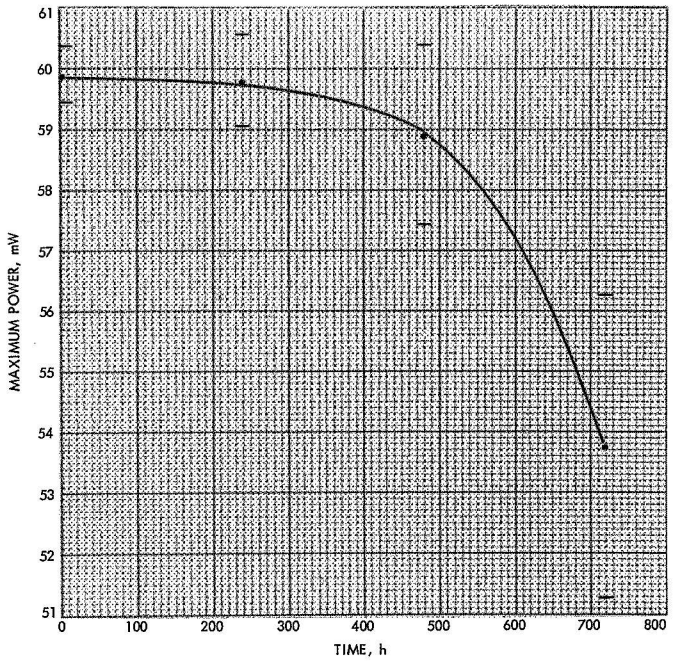

Fig. A-16. Maximum power as a function of exposure time, M cells (Heliotek Ti–Ag, soldered)

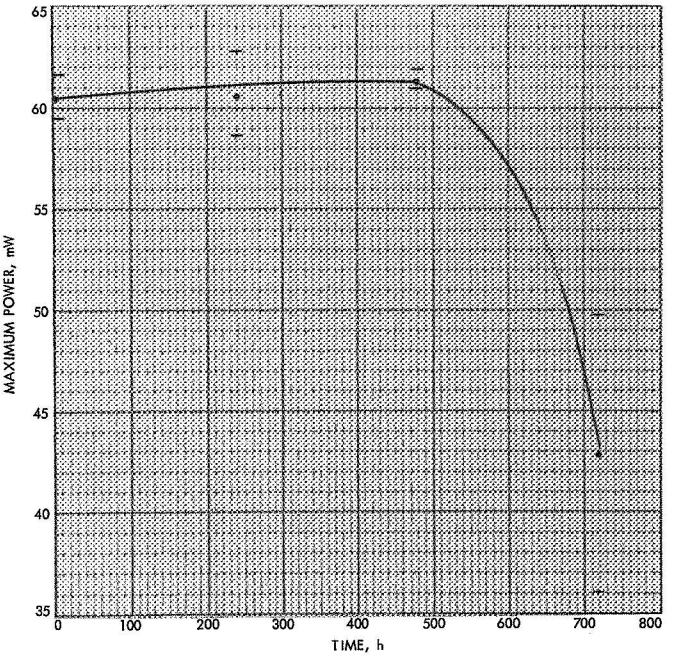

Fig. A-17. Maximum power as a function of exposure time, HP cells (Heliotek Ti–Pd–Ag, solderless)

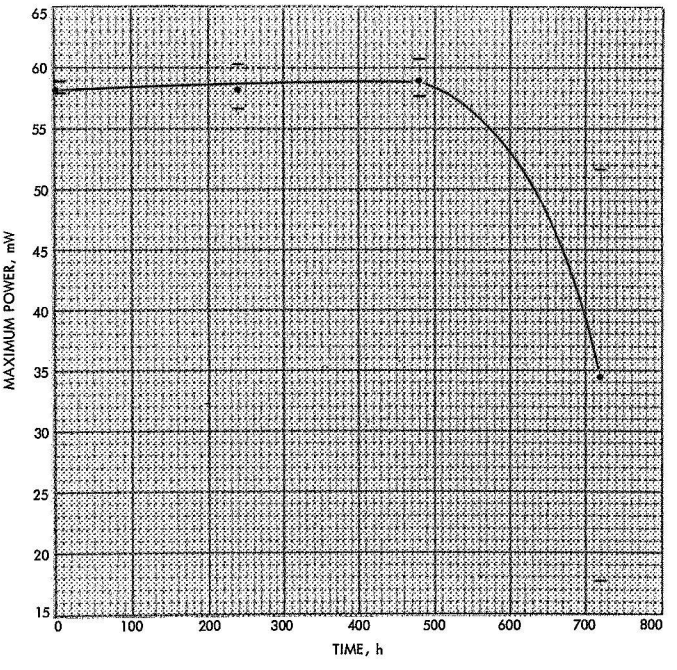

Fig. A-18. Maximum power as a function of exposure time, CP cells (Centralab Ti–Pd–Ag, solderless)

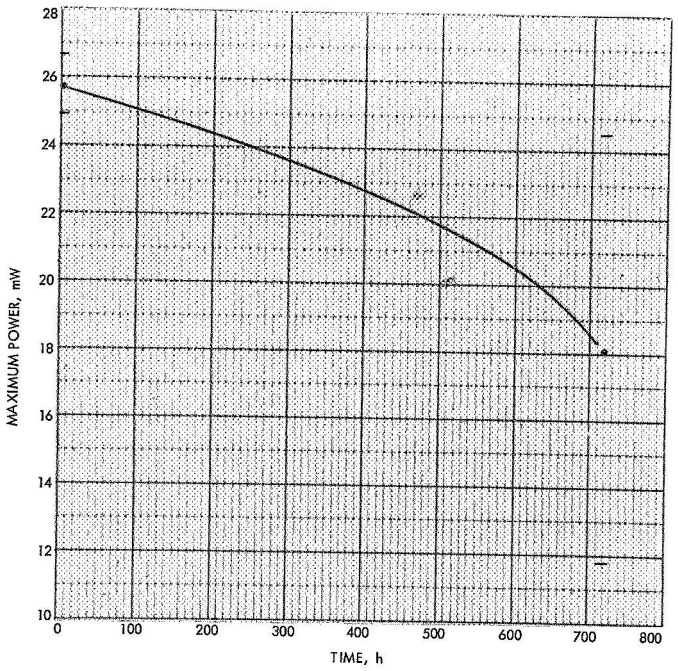

Fig. A-19. Maximum power as a function of exposure time, TL cells (Texas Instruments Ti–Ag, solderless, lithium-doped)

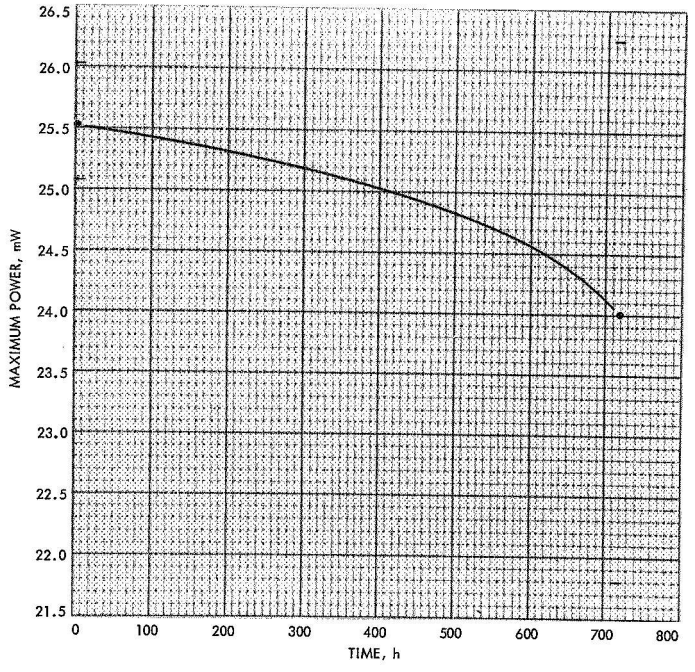

Fig. A-20. Maximum power as a function of exposure time, HL cells (Heliotek Ti–Ag, solderless corner dart contacts, lithium-doped)

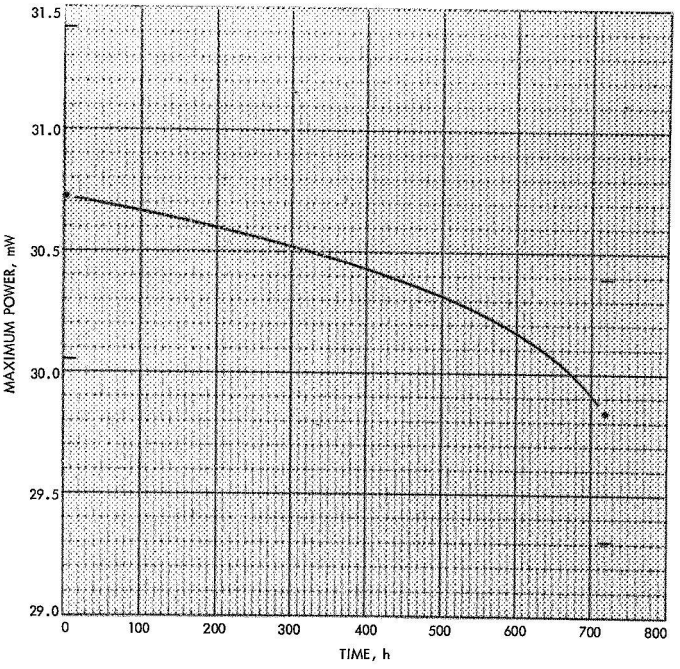

Fig. A-21. Maximum power as a function of exposure time, CL cells (Centralab Ti–Ag, solderless, lithium-doped)

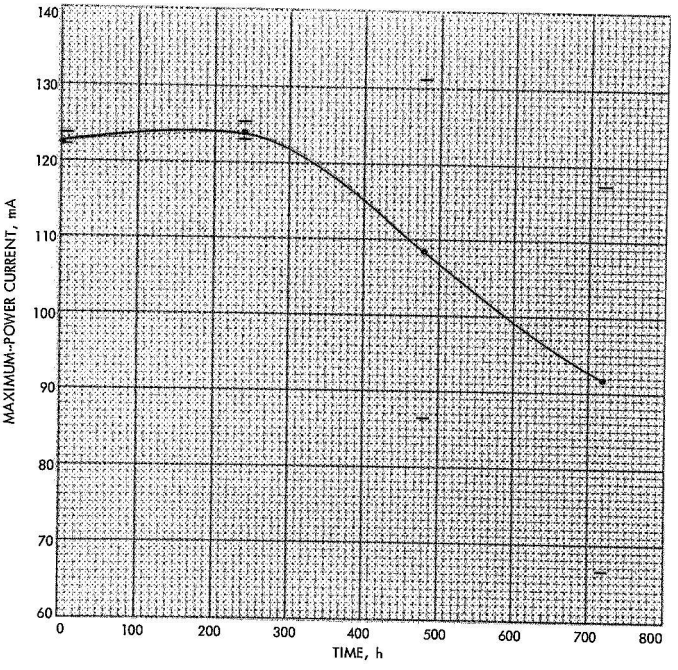

Fig. A-22. Maximum-power current as a function of exposure time, H cells (Heliotek Ti–Ag, solderless)

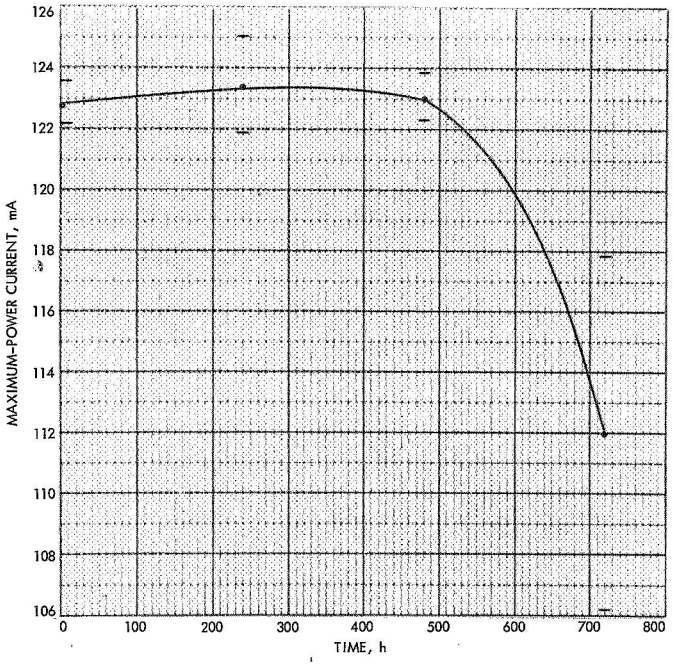

Fig. A-23. Maximum-power current as a function of exposure time, M cells (Heliotek Ti–Ag, soldered)

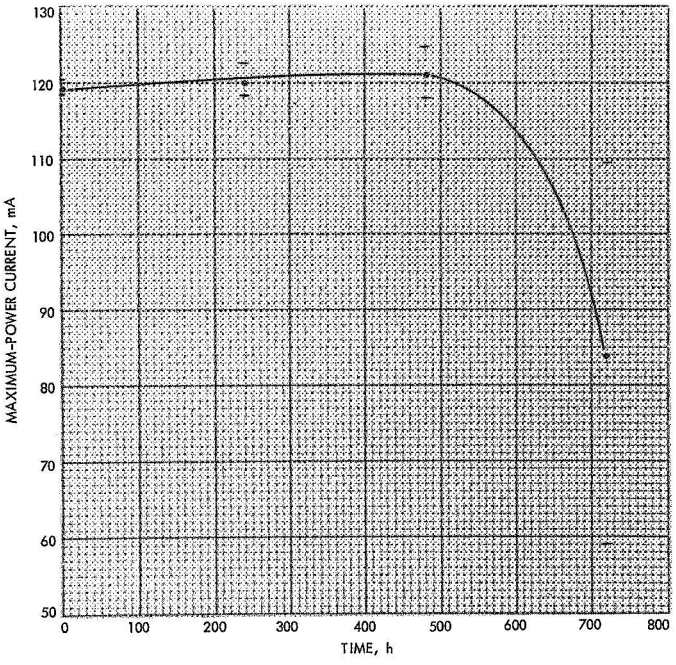

Fig. A-25. Maximum-power current as a function of exposure time, CP cells (Centralab Ti–Pd–Ag, solderless)

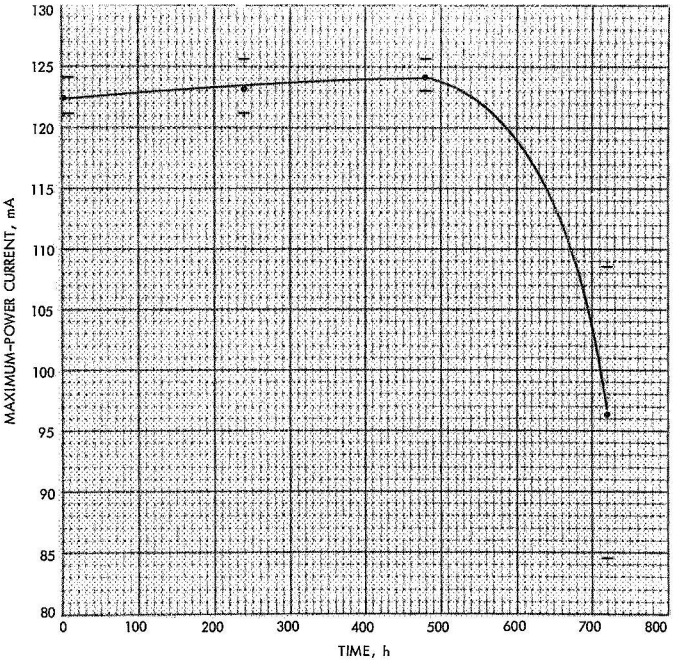

Fig. A-24. Maximum-power current as a function of exposure time, HP cells (Heliotek Ti–Pd–Ag, solderless)

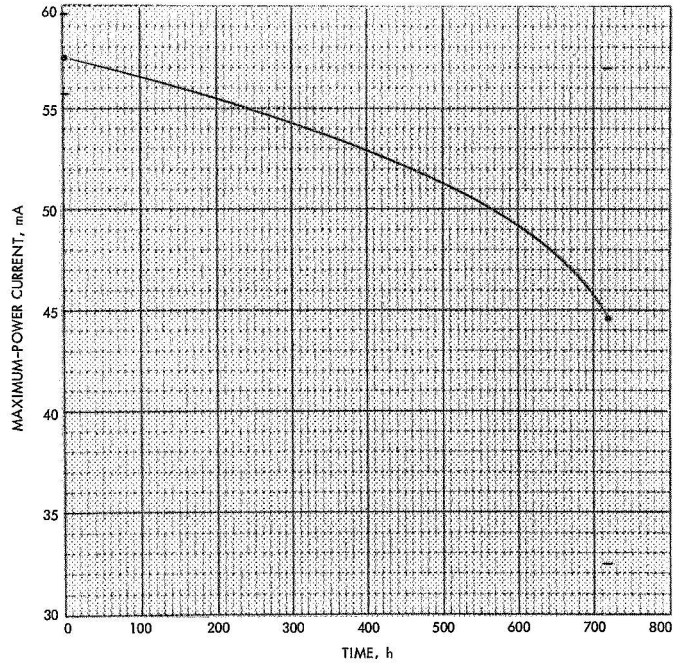

Fig. A-26. Maximum-power current as a function of exposure time, TL cells (Texas Instruments Ti–Ag, solderless, lithium-doped)

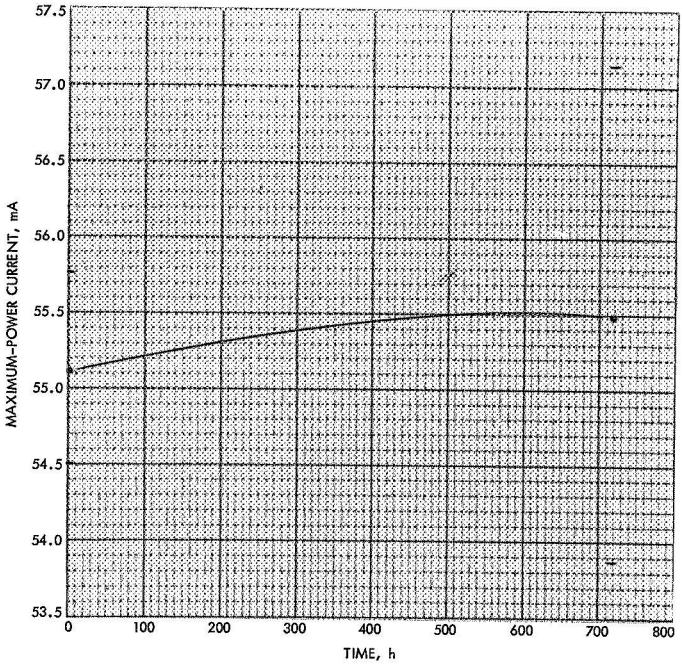

Fig. A-27. Maximum-power current as a function of exposure time, HL cells (Heliotek Ti–Ag, solderless corner dart contacts, lithium-doped)

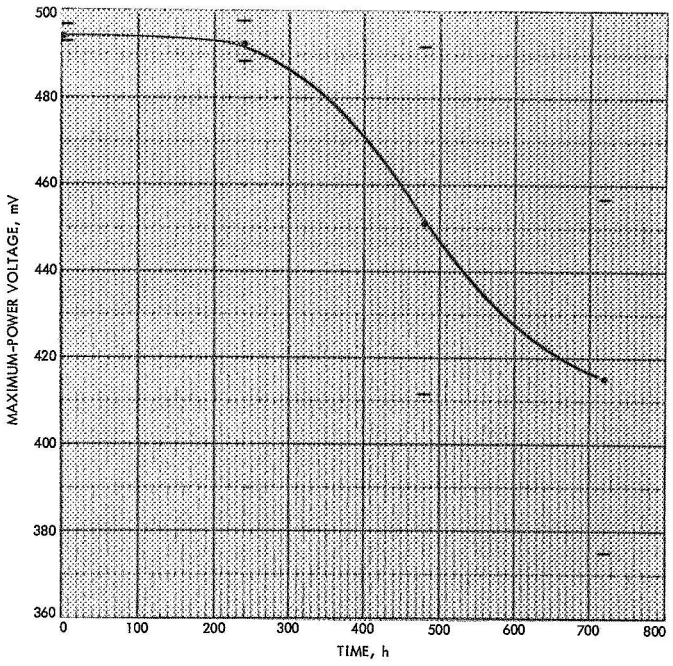

Fig. A-29. Maximum-power voltage as a function of exposure time, H cells (Heliotek Ti–Ag, solderless)

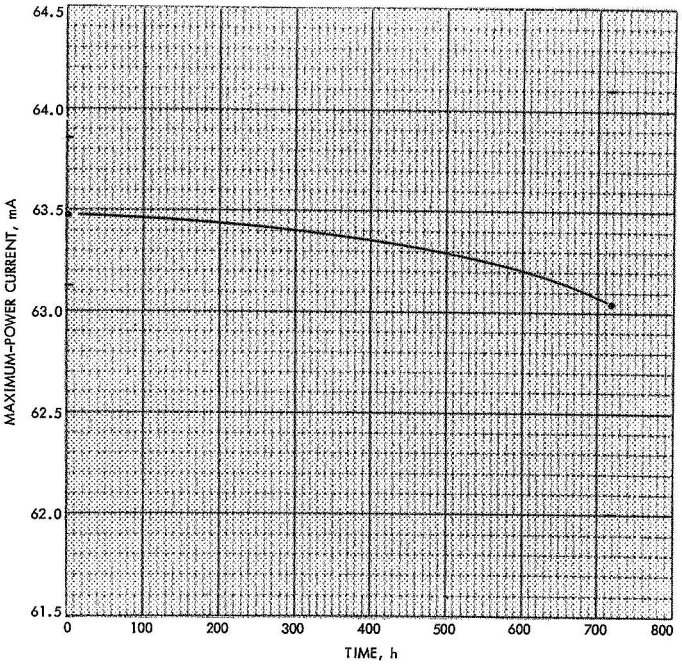

Fig. A-28. Maximum-power current as a function of exposure time, CL cells (Centralab Ti–Ag, solderless, lithium-doped)

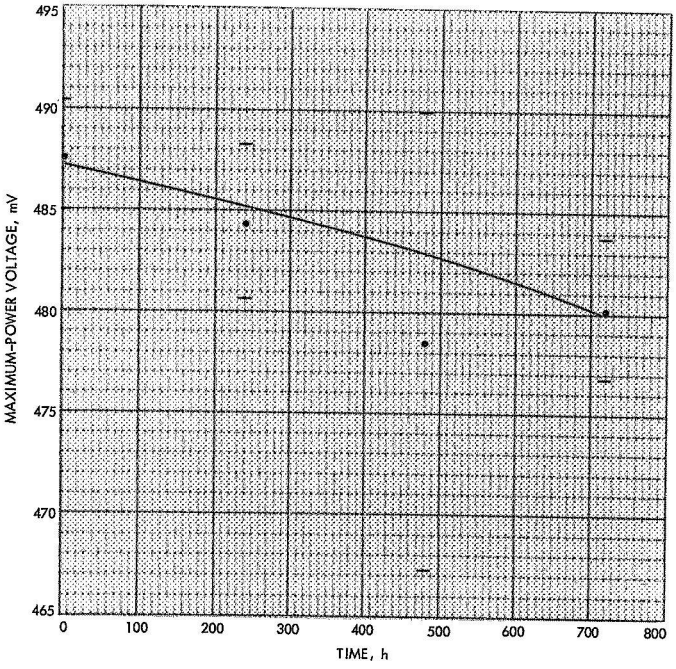

Fig. A-30. Maximum-power voltage as a function of exposure time, M cells (Heliotek Ti–Ag, soldered)

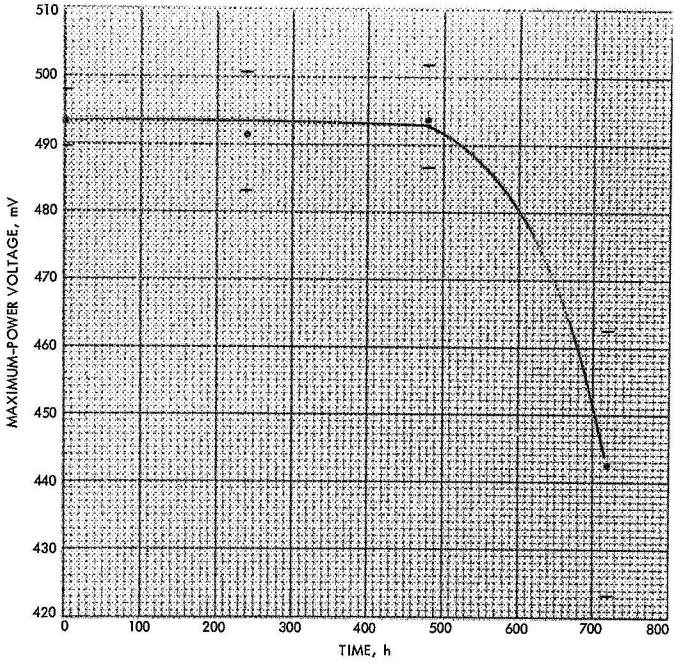

Fig. A-31. Maximum-power voltage as a function of exposure time, HP cells (Heliotek Ti–Pd–Ag, solderless)

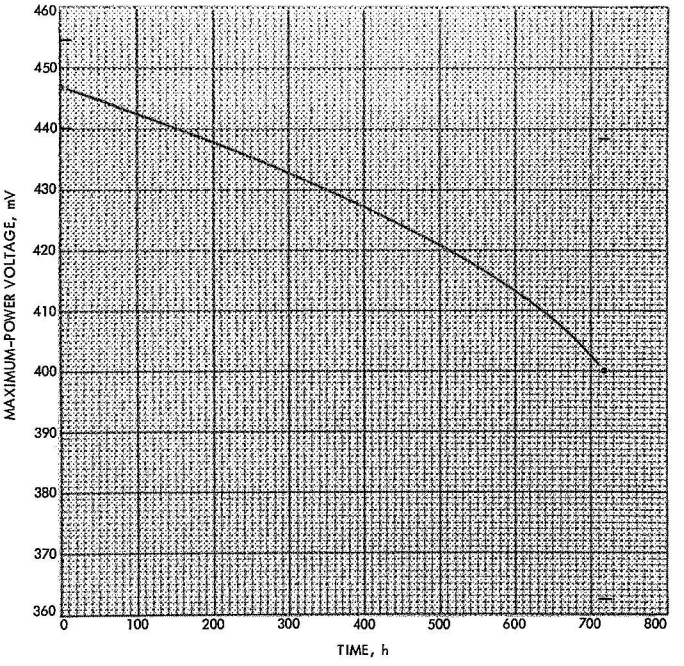

Fig. A-33. Maximum-power voltage as a function of exposure time, TL cells (Texas Instruments Ti–Ag, solderless, lithium-doped)

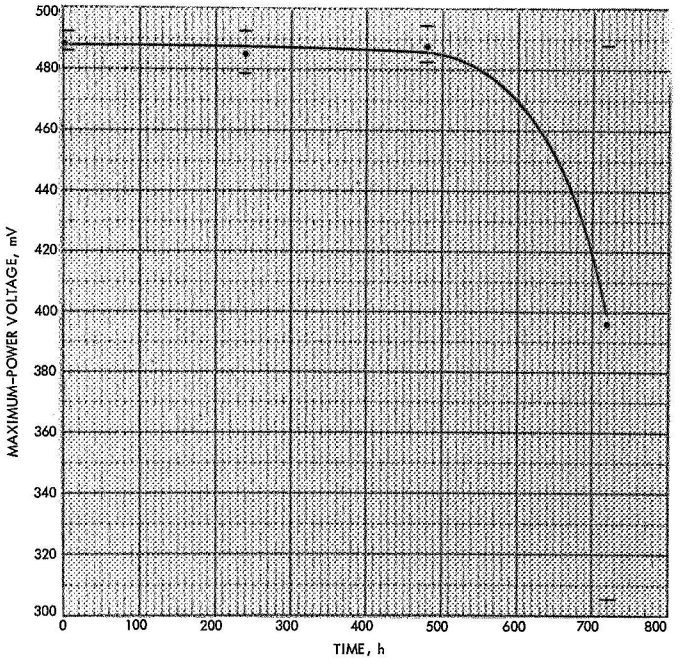

Fig. A-32. Maximum-power voltage as a function of exposure time, CP cells (Centralab Ti–Pd–Ag, solderless)

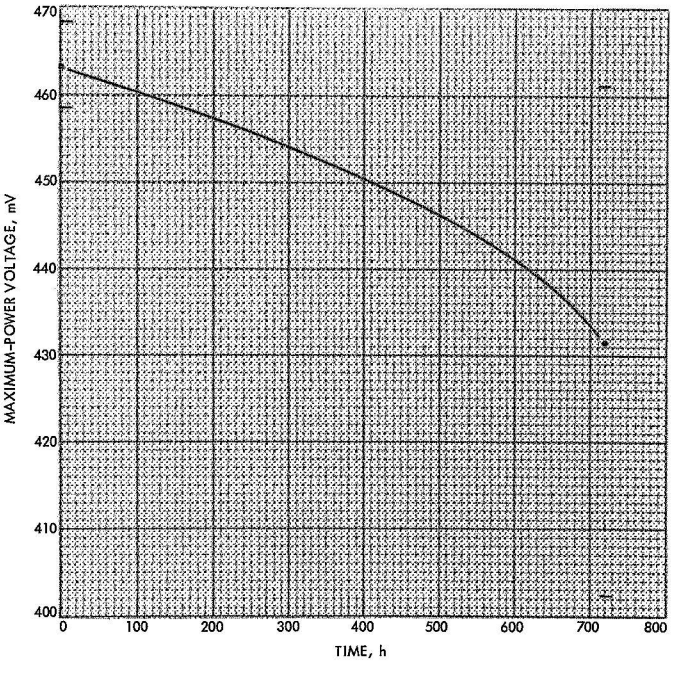

Fig. A-34. Maximum-power voltage as a function of exposure time, HL cells (Heliotek Ti–Ag, solderless corner dart contacts, lithium-doped)

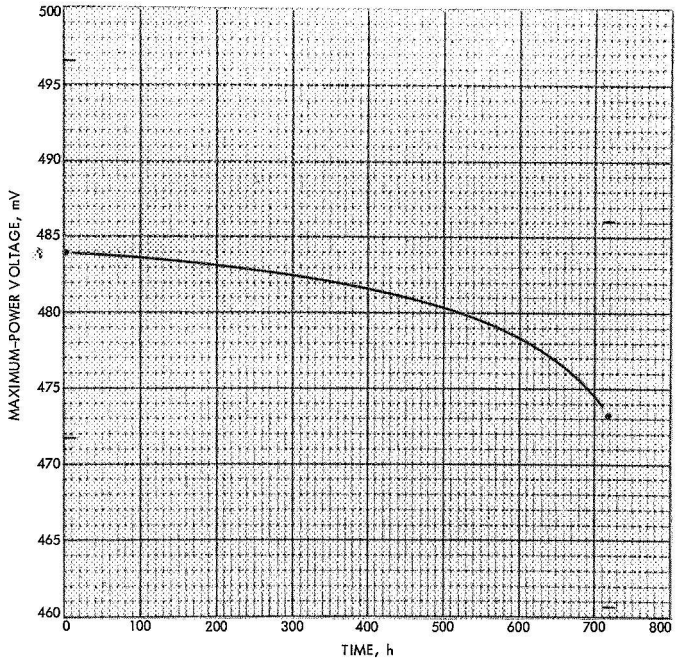

Fig. A-35. Maximum-power voltage as a function of exposure time, CL cells (Centralab Ti–Ag, solderless, lithium-doped)

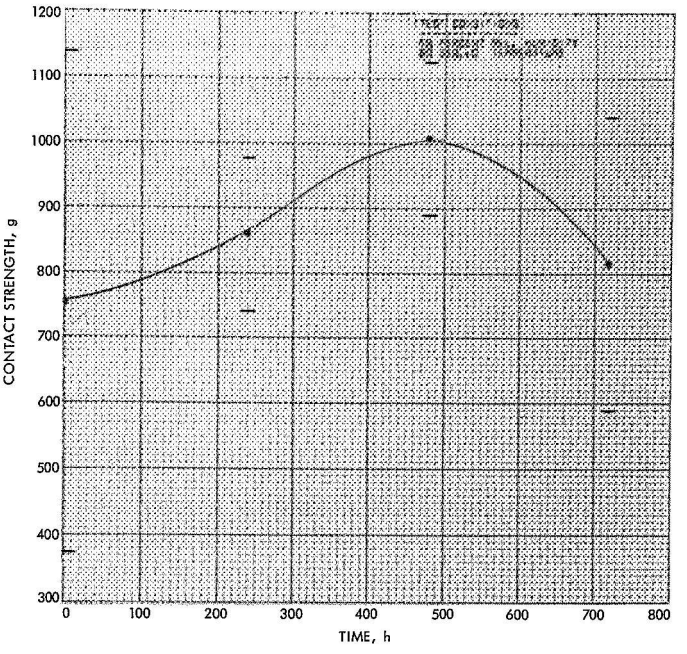

Fig. A-37. Strength of *n*-contact as a function of exposure time, M cells (Heliotek Ti–Ag, soldered)

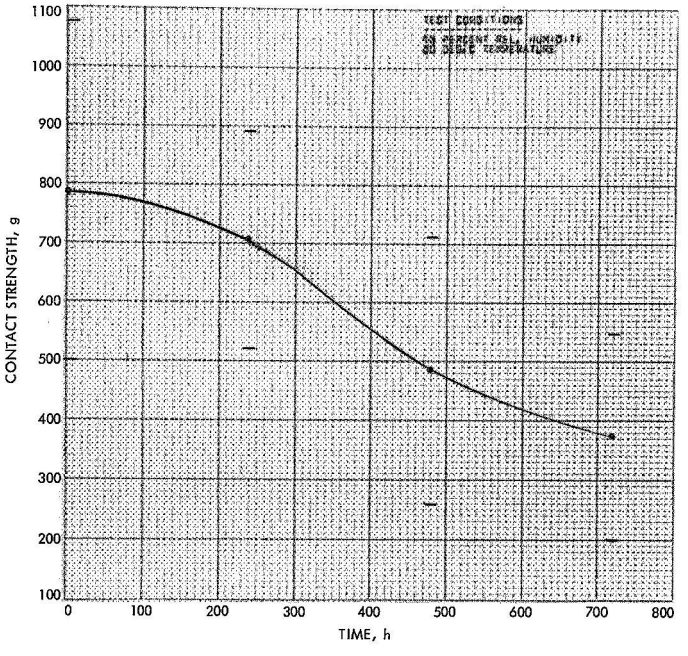

Fig. A-36. Strength of *n*-contact as a function of exposure time, H cells (Heliotek Ti–Ag, solderless)

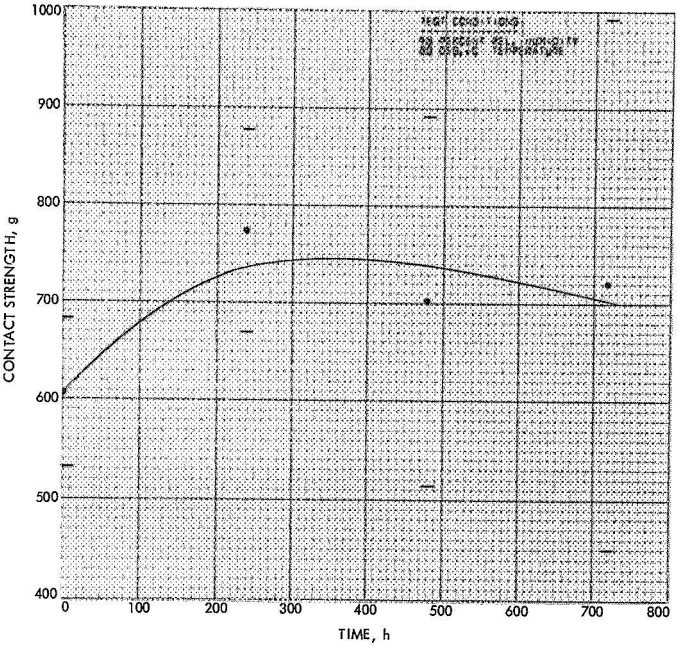

Fig. A-38. Strength of *n*-contact as a function of exposure time, HP cells (Heliotek Ti–Pd–Ag, solderless)

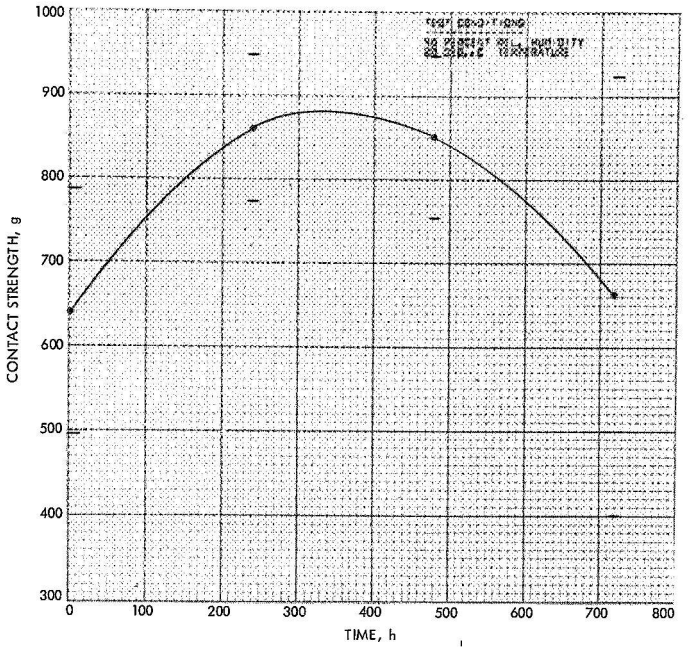

Fig. A-39. Strength of *n*-contact as a function of exposure time, CP cells (Centralab Ti–Pd–Ag, solderless)

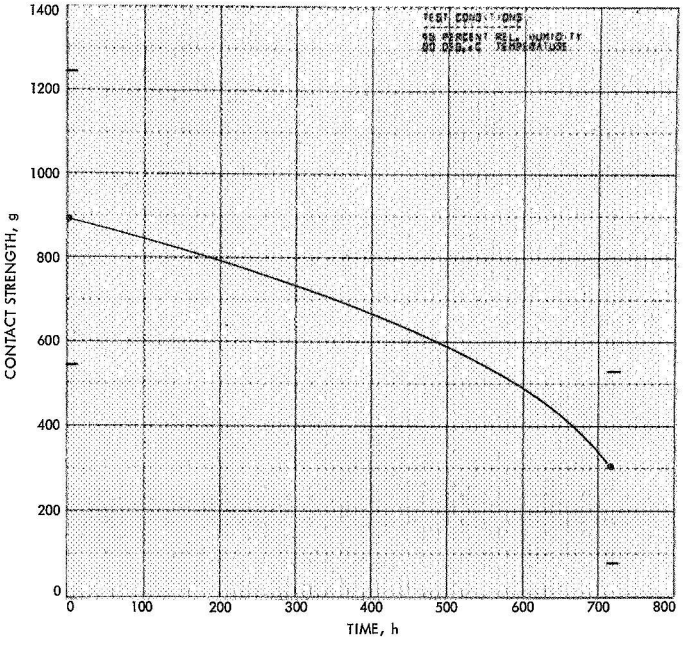

Fig. A-40. Strength of *n*-contact as a function of exposure time, TL cells (Texas Instruments Ti–Ag, solderless, lithium-doped)

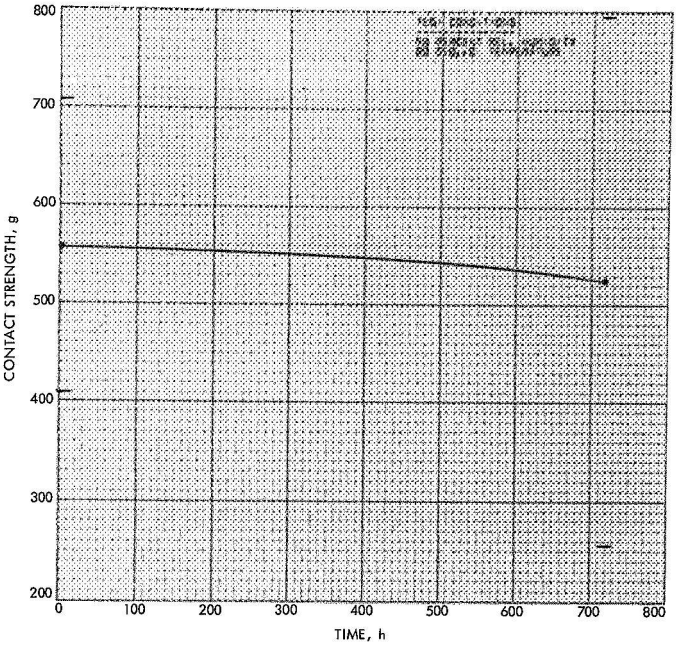

Fig. A-41. Strength of *n*-contact as a function of exposure time, HL cells (Heliotek Ti–Ag, solderless, lithium-doped)

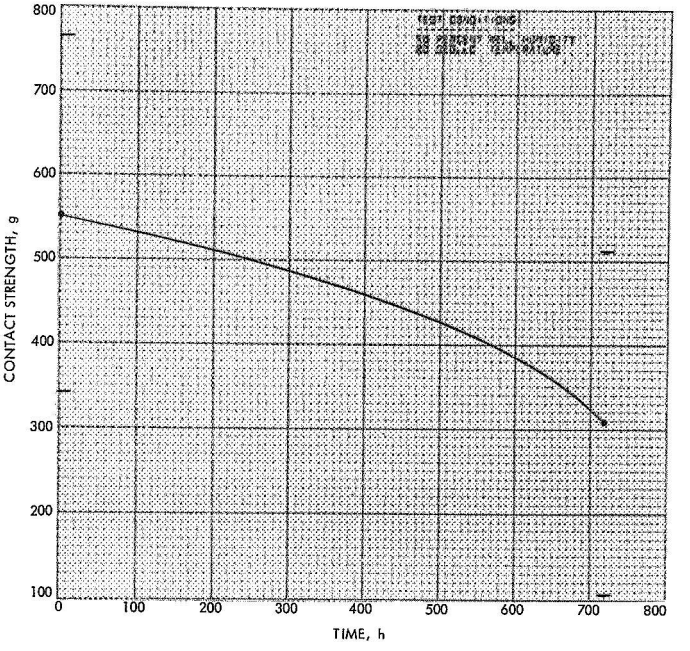

Fig. A-42. Strength of *n*-contact as a function of exposure time, CL cells (Centralab Ti–Ag, solderless, lithium-doped)

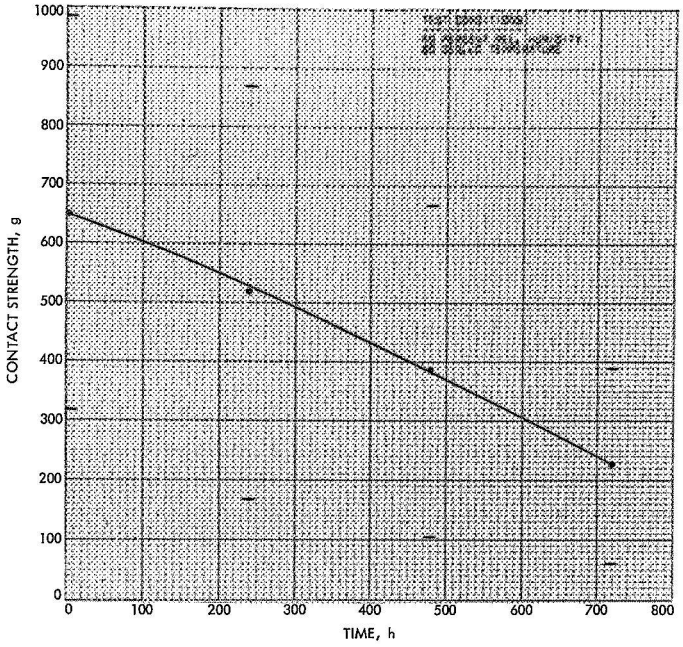

Fig. A-43. Strength of *p*-contact as a function of exposure time, H cells (Heliotek Ti–Ag, solderless)

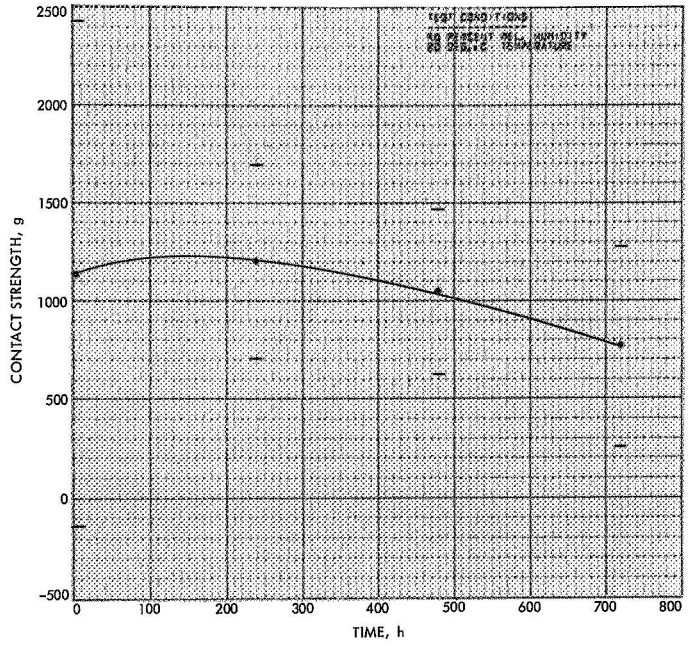

Fig. A-44. Strength of *p*-contact as a function of exposure time, M cells (Heliotek Ti–Ag, soldered)

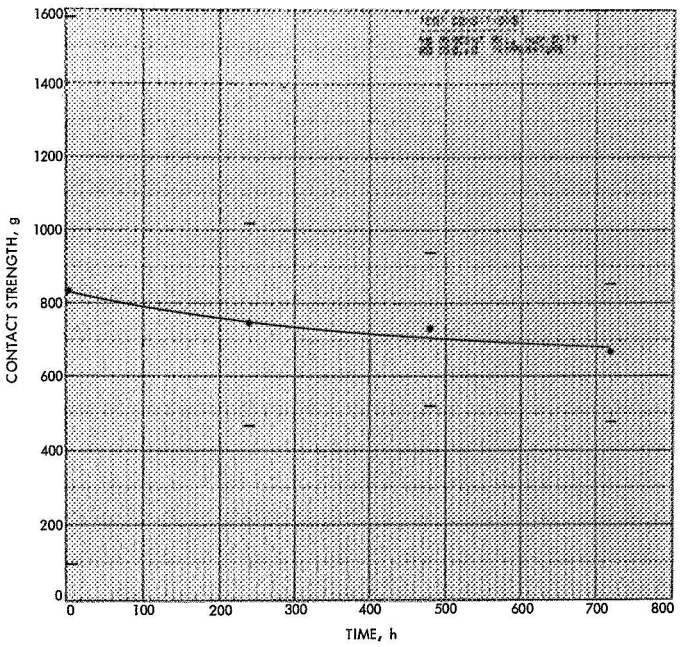

Fig. A-45. Strength of *p*-contact as a function of exposure time, HP cells (Heliotek Ti–Pd–Ag, solderless)

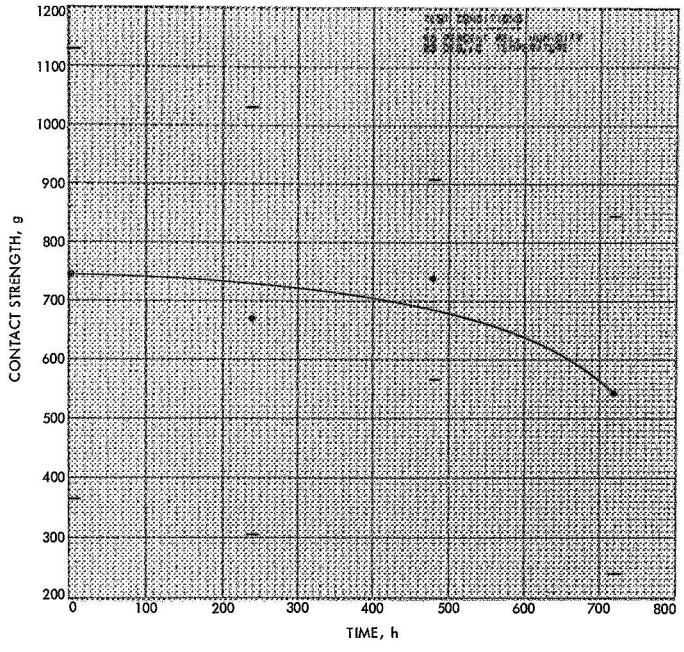

Fig. A-46. Strength of *p*-contact as a function of exposure time, CP cells (Centralab Ti–Pd–Ag, solderless)

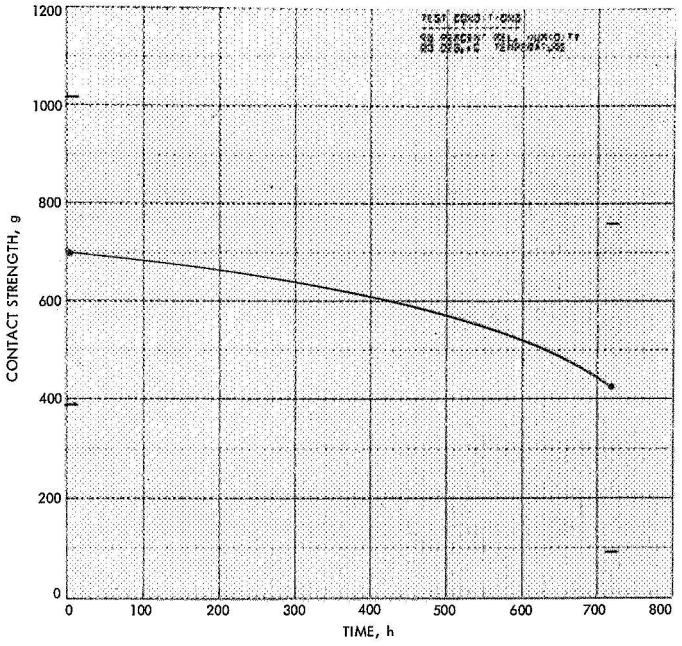

Fig. A-47. Strength of *p*-contact as a function of exposure time, TL cells (Texas Instruments Ti–Ag, solderless, lithium-doped)

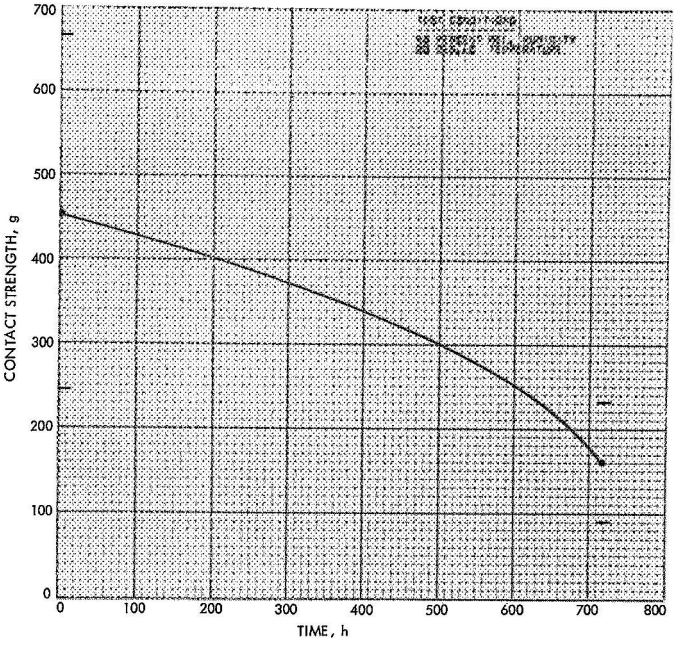

Fig. A-48. Strength of *p*-contact as a function of exposure time, CL cells (Centralab Ti–Ag, solderless, lithium-doped)